Dynamic modeling and control of a two wheeled robotic vehicle with a virtual payload

Article · March 2011

3 authors:

Khaled Goher
University of Lincoln
62 PUBLICATIONS **229** CITATIONS
SEE PROFILE

Mohammad Osman Tokhi
The University of Sheffield
559 PUBLICATIONS **4,372** CITATIONS
SEE PROFILE

Nazmul Siddique
Ulster University
120 PUBLICATIONS **924** CITATIONS
SEE PROFILE

VOL. 6, NO. 3, MARCH 2011 ISSN 1819-6608
ARPN Journal of Engineering and Applied Sciences


www.arpnjournals.com

DYNAMIC MODELING AND CONTROL OF A TWO WHEELED ROBOTIC VEHICLE WITH A VIRTUAL PAYLOAD

K. M. Goher[1], M. O. Tokhi[2] and N. H. Siddique[3]
[1]Department of Mechanical and Industrial Engineering, College of Engineering, Sultan Qaboos University, Oman
[2]Department of Automatic Control and Systems Engineering, The University of Sheffield, United Kingdom
[3]School of Computing and Intelligent Systems, University of Ulster, United Kingdom
E-Mail: kgoher@squ.edu.om

ABSTRACT

One of the challenging issues to consider in balancing a two-wheeled robotic machine (TWRM) is when the load carried by the machine is changing position along the vehicle intermediate body (IB). An issue of interest in this case is the resulting impact on the system behaviour due to changing position of the load. Further complications arise with changing the size of the load. This work presents investigations into controlling a TWRM with a payload positioned at different locations along its IB. Two types of control techniques are developed and implemented on the system, the traditional proportional-derivative (PD) control and fuzzy logic (FL) control. PD and PD-fuzzy logic control techniques are developed to balance the vehicle with a payload incorporating two different scenarios. Firstly, the payload is positioned at different locations along its IB. Secondly, it is considered to perform a continuous sliding motion along the IB. The balancing of the robot has to be achieved during the motion of the vehicle and the payload along the IB. An external disturbance force is applied to the rod which constitutes the IB in order to test the robustness of the developed controllers. Investigations are carried out on the effect of changing the level and duration of the disturbance force, and changing the speed of the payload on the system during the balancing mode. Simulation results of both control algorithms are analyzed on a comparative basis.

Keywords: wheeled robot, dynamic modeling, FL control, PD control, inverted pendulum.

1. INTRODUCTION

The research on balancing two-wheeled robots has gained momentum over the last decade in a number of robotics laboratories around the world. This is due to the inherent unstable dynamics of such systems. The control quality of such robots is characterized by the ability to balance on its two wheels and provide spin on the spot. This additional maneuverability allows easy navigation on various terrains, turn at sharp corners and traverse small steps or curbs. These capabilities have the potential to solve a number of challenges in the industrial and public sectors. For example, a motorized wheelchair utilizing this technology would give the operator greater maneuverability and thus access to places most able-bodied people take for granted. Small carts built utilizing this technology allow humans to travel short distances in a small area or factories as opposed to using cars or buggies which are more polluting. The rapid increase of the aged population in countries like Japan has prompted researchers to develop robotic wheelchairs to assist an elderly to move around (Takahashi *et al*., 2000).

Mobile wheeled inverted pendulum models have evoked a lot of interest recently and at least one commercial product, Segway [28]. Such vehicles are of interest because they have small footprint and possess high navigation capabilities. There are many robots without manipulation capabilities that balance around two wheels such as JOE robot [29]. The nature of this two-wheeled vehicle poses several interesting control questions. For instance, while a person occupies the vehicle, his/her mass changes the centre of gravity of the vehicle which in turn has an impact on the control technique used. One of the recent challenges in such applications is the development of control schemes to help a disabled or an elderly person on a two wheeled wheelchair [30] to move to further levels in shopping centers or to have eye to eye contact with others. Industrial applications of such vehicles will arise to a great extent in the coming years; for instance, material handling in narrow paths to different heights etc (Goher and Tokhi, 2008).

The idea of balancing a robot on two wheels is based on the concept of inverted pendulum model. This model has been widely used by researches around the world in controlling not only wheeled robots but other types of robot as well such as legged robots. In recent years, researchers have applied the idea of a mobile inverted pendulum model to various problems like designing walking gaits for humanoid robots, robotic wheelchairs and personal transport systems.

In the work carried out by Shiroma *et al*., (1996) on 'Cooperative behaviour of a wheeled inverted pendulum for object transportation', the interaction of forces between objects and the robot has been shown by taking into account the stability effects due to these forces. Ooi (2003) implemented an indirect Kalman filter configuration combining a piezo rate gyroscope sensor and an inclinometer to obtain an accurate estimate of the tilt angle and its derivative. He examined the suitability of linear control systems like the linear quadratic regulator and pole-placement controller in stabilising the system. Browning (2004) presented a new domain, called Segway Soccer, for investigating the coordination of dynamically formed, mixed human-robot teams within the realm of a team task that requires real-time decision making and

response. Salerno and Angeles, (2004), presented a multivariable control by differentiable state feedback of semi-autonomous self-balancing two-wheeled quasi-holonomic robots. The analysis of robot stability, based on the Lyapunov linearization method, was provided as well. Pathak (2005) analyzed the dynamic model of a wheeled inverted pendulum (e.g., Segway, Quasimoro, and Joe) from a controllability and feedback lineariability point of view. Kim (2005) discussed the enhancement of floor-driving ability of a two wheeled inverted-pendulum-type autonomous vehicle based on the dynamics of the robotic mechanism using Kane's dynamic modeling. Randal (2005) applied the idea of non-linear control strategy, where two types of semiconductor sensors were used to provide tilt information to the robot to balance. The sensors used were gyroscopes and accelerometer.

Most of the previously mentioned works showed the practical validity of the robot from controllability perspective. However, not much work on the dynamics of this kind of robot has been reported. One of the most important contributions discussing the dynamics of two-wheeled inverted pendulum robot is the work carried by Kim (2005). The exact dynamics have been investigated in order to provide necessary information for further design and production. Tsai (2006) developed techniques for system design, modeling and adaptive control of a personal two-wheeled transporter driven by two DC servomotors. A mechatronic system structure for the vehicle was described and its mathematical modeling incorporating the friction between the wheels and motion surface was derived as well. Two adaptive two-degrees-of-freedom (DOF) controllers were designed to achieve self-balancing and rotation control. Experimental results revealed that the proposed controllers were capable of providing appropriate control actions to steer the vehicle in a desired manner. Hu and Tsai (2006) investigated robust motion pilot control of an auto-balancing two-wheeled cart where the feedback control system was solely based on the angle of inclination without using any velocity information. H∞ control was employed to design a robust stabilizing controller.

The type of intelligent robot proposed in this work is a mobile robot with a two-wheeled inverted pendulum. This design was chosen because its mechanism has an innately clumsy motion for stabilizing the robot's body posture. The robot has a body with two wheels for moving in a plane and a head similar to a human head for controlling the motion. Two independent driving wheels are used for position control, for fast motion in a plane without casters. Two-wheeled machines have different applications due to their advantages which arise from their special design. For example, a two wheeled vehicle may be safer for the occupants while simultaneously being more agile to navigate narrow city streets. Furthermore, the reduced volume and lower mass of this configuration would increase fuel efficiency and overall functionality. However, because such a vehicle would be inherently unstable it would require an intelligent control mechanism to provide dynamic balancing.

The aforementioned researches have concentrated on developing control algorithms to keep the two-wheeled inverted pendulum robot in a balancing state. Other works have discussed the dynamics of the system. All these works have considered a fixed position for the load, which is mainly the global mass of the robot or the rod attached to the axle of the driving wheels. The load is considered to be concentrated at the centre of mass (COM) of the whole system. The work presented in this paper considers challenging control solutions of balancing a two-wheeled robotic machine with changing position and size of the load.

A system with two-wheeled vehicle is considered to be highly non linear and under actuated. Such systems are considered to be utilized for outdoor environmental usage where many unexpected conditions could apply to the vehicle and affect its performance. These include the presence of sources of disturbances such as sudden impact forces or obstacles during maneuvering of the vehicle. The uncertainties due to such effects need to be considered when designing control strategies for outdoor machines. Poorly modeled behaviour of loads carried by the vehicle is another issue which needs to be considered when dealing with such systems. The aim of this work is to develop a simple, effective and robust control approach capable of balancing a TWRM under the effect of a disturbance force varying in magnitude, position and duration. The control scheme needs to be able to cope with changes in the speed and position of an attached payload. Furthermore, an investigation of the impact of changing the length of the intermediate body is considered in this study.

The rest of the paper is organized as follows: Section 2 describes the system dynamics considering a disturbance effect applied to the IB and the frictional resistance at the joint connecting the wheel axle and the IB. Section 3 proposes a control strategy utilizing a conventional PD control scheme to test the vehicle model under certain varying dynamic conditions followed by an implementation of a PD-like fuzzy control approach for further investigation of a suitable control scheme. A numerical simulation analysis is carried out in section 4 based on the two suggested control techniques. The paper is concluded in section 5 highlighting the achievements of the work.

2. MODELING OF THE TWRM

The TWRM system considered in this work comprises a rod on an axle incorporating two wheels as described in Figure-1. The robot is powered by two DC motors driving the vehicle wheels. A payload is attached to the IB of the vehicle. This payload is considered to act at different positions along the IB in static and dynamic manners. The payload is considered to simulate the weight of a person on a wheelchair or an object to be handled to different heights if a manual handling task is given to the robot. Rigid body dynamics are assumed in this study. A reference Cartesian coordinate frame designated as $OXYZ$ attached to the axle connecting the wheels with its origin

located at the vehicle centre point O as shown in Figure-1 is used for the angular and translational motion of the vehicle. The $Z-$axis points vertically upward, the $X-$axis is parallel and coincides with the axle of the wheels, and the $Y-$axis is determined according to the right-hand rule in the rectangular coordinate system. The IB is considered to be balanced if it coincides with the positive $Z-$axis. Partial angular deviation from the $Z-$axis causes an imbalance for the vehicle with a tilt angle θ_P from the $Z-$axis. The two main dynamic modes of the vehicle which will be considered in both the mathematical modelling and control processes are the angular deflection of the IB from the $Z-$axis and the linear motion of the entire system in the $Y-$direction.

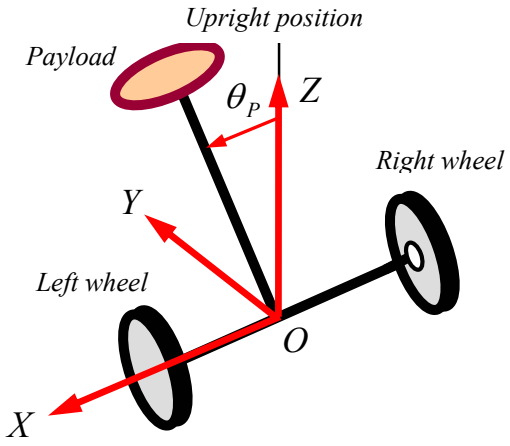

Figure-1. Schematic diagram of the two-wheeled vehicle.

The pendulum and wheel dynamics are initially analyzed separately, and this will eventually lead to two equations of motion which completely describe the behaviour of the TWRM. Consider Figure-2, which represents the free body diagrams of the right and left wheels of the robot, where H_{FR} and H_{FL} are the frictional forces between the wheel and the surface. H_{TR}, H_{TL}, V_{TR} and V_{TL} are the horizontal and vertical reaction forces respectively. H_R, H_L, P_R, P_L are the horizontal and vertical reaction forces between the IB and the wheel axle at the connecting joint.

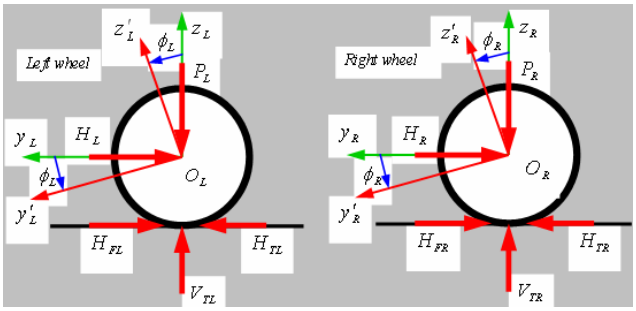

Figure-2. Free body diagrams of the vehicle wheels.

2.1 Dynamic model of TWRM

The dynamic model of the system is described in this section by introducing the governing differential equations describing the dynamics of the two-wheeled vehicle. The model is derived based on the Newton-Euler equations of motion. The dynamic model of the entire system consists of two separate sub-models, namely: the non-linear model of the inverted pendulum and a linear model of the permanent magnet direct current motor activating the wheels.

The dynamics of vehicle wheels and intermediate body are initially analysed separately and this will lead to the following two non-linear equations of motion. The tilt angle acceleration $\ddot{\theta}_P$ and vehicle acceleration $\ddot{Y}$, describing the main two dynamic behaviours of the TWRM, are obtained as

$$\ddot{\theta}_P = \frac{1}{\left(I_{eq}+\left(M+M_p\right)L_g^2\right)}\left(-\frac{k_m k_e}{RR_w^2}\left(\dot{y}_L+\dot{y}_R\right)+\frac{k_m}{RR_w}\left(V_L+V_R\right)+M_F\right.$$
$$\left.-\left(M+M_P\right)L_g g\sin\theta_p+\left(M+M_P\right)L_g\ddot{Y}\cos\theta_p+F\cos\theta_P\left(S-2L_g\right)\right) \quad (1)$$

and

$$\ddot{Y} = \frac{1}{\left(2\left(M_w+\frac{J_{wy}}{R_w^2}\right)+\left(M+M_p\right)\right)}\left(-\frac{k_m k_e}{RR_w^2}\dot{Y}+\frac{k_m}{RR_w}\left(V_L+V_R\right)\right.$$
$$\left.-\left(M+M_P\right)L_g\ddot{\theta}_p\cos\theta_p+\left(M+M_P\right)L_g\dot{\theta}_p^2\sin\theta_p-F\right) \quad (2)$$

Definition of the variables and constants is given in the nomenclature. The applied terminal voltage V_L and V_R of the left and right wheels are defined in terms of motor torques T_L and T_R as follows:

$$V_L = \frac{R}{k_m}\left(T_L + \frac{k_m k_e}{RR_w}\dot{y}_L\right) \quad (3)$$

$$V_R = \frac{R}{k_m}\left(T_R + \frac{k_m k_e}{RR_w}\dot{y}_R\right) \quad (4)$$

The final torque required for the tilt angle acceleration $\ddot{\theta}_P$ and linear vehicle acceleration $\ddot{Y}$ is expressed as

$$V_L + V_R = \frac{R}{k_m}\left(T_L + \frac{k_m k_e}{RR_w}\dot{y}_L\right) + \frac{R}{k_m}\left(T_R + \frac{k_m k_e}{RR_w}\dot{y}_R\right) \quad (5)$$

Detailed descriptions of linear model of the DC motors, non-linear model of the wheels and the IB dynamics are provided in the Appendix.

3. CONTROL STRATEGY

The intermediate body is considered to be balanced at the upright position if it coincides with the positive Z–axis. Partial angular deviation from the Z–axis causes an imbalanced mode for the vehicle with a tilt angle θ_P from the $Z-$axis. The main two dynamic activities of the vehicle which will be considered in both the mathematical modelling process and implementation of the control technique for the angular deflection of the IB from the $Z-$axis and the linear motion of the entire system in the $Y-$direction. The IB is considered initially in the upright position; $\theta_P = 0$. With a disturbance force F_d applied to the rod, the IB will move from the upright position with an angle, measured from that position, directly proportional to the magnitude and direction of the disturbance force.

The control strategy is based on minimizing the error between the actual angular position θ_m of the IB and the desired (stable) angular position θ_d, which is zero. The two control signals resulting from both feedback loops are added to constitute the control signal in terms of the motor terminal voltage required to balance the vehicle at the target position (Figure-A2 in the appendix).

The control algorithm is implemented first using a conventional PD controller, shown in Figure-3, for testing the model. For purposes of comparison, the process is repeated using a PD-like fuzzy control algorithm, as shown in Figure-4. For both control strategies, the measured error and its rate of change for both the IB tilt angle and the vehicle position are used as control inputs, while the controller output is the required motor terminal voltage V_a.

The PD controller parameters were tuned using a trial and error method to achieve a desired system performance. A disturbance force F_d is applied on the IB after 10 seconds from the start of the simulation and then at each 90 second interval. This interval was chosen as a safe limit for repeating such impact forces to the IB. Below such limit, it was found that the developed controller would not completely keep the IB at a stable position and result in an accumulated error in the corresponding measurements.

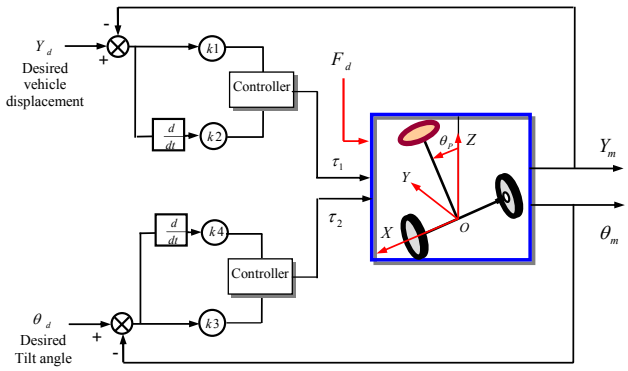

Figure-3. Implementation of a PD control strategy.

3.1 Fuzzy control of TWRM

Conventional control techniques require accurate mathematical models to describe the dynamics of the system under study. One of the major limitations of conventional control systems is their inability to cope with changes in the plant dynamics with time and actuator saturation, which add to the nonlinearity of the system (Lin *et al*., 1996). These techniques result in tracking error, when the payload varies fast, and overshoot during transients. An interesting alternative that could be investigated is the use of fuzzy logic control (FLC) methods (Mamdani and Assilian, 1975, Zadeh, 1965, 1973). In recent years, FLC has attracted considerable attention as a tool for novel control approaches because of the variety of advantages that it offers over classical control techniques (Zadeh, 1973). The FLC paradigm has been developed as an alternative to conventional model-based control systems (Mamdani, 1974). It does not require a mathematical model of the plant and can be applied equally to linear and nonlinear systems.

It is evident that human knowledge is becoming more and more important in control systems design due to the fact that many industrial processes are highly nonlinear and have un-modeled plant dynamics and uncertainties. This experiential perspective in controller design requires the acquisition of heuristic and qualitative, rather than quantitative, knowledge or expertise from the human operator. During the past several years, fuzzy control has emerged as one of the most active and powerful areas for research in the application of such nonlinear real world systems using fuzzy set theory (Zadeh, 1973). Fuzzy control approach has been applied very successfully in practical problems, especially when conventional control techniques do not yield satisfactory performance. The great advantage of fuzzy controllers is the ability to introduce the knowledge of human experts about proper and correct control of a plant in the controller (Piegat, 2001, 2006; von Alrrock, 1995).

Fuzzy-based control has been used extensively in the field of inverted pendulum-like machines and wheeled robotic machines. Shi *et al*., (2004) implemented a predictive fuzzy control technique on a two wheeled robot for navigation. Hladek (2007) designed and implemented a multi-agent fuzzy expert system for robotic soccer control. Astudillo *et al*., (2006) developed a tracking controller for the dynamic model of unicycle mobile robot, based on fuzzy logic theory, by integrating a kinematic controller and a torque controller. Maravall *et al*., (2005) constructed a hybrid fuzzy control system that incorporates PD control into a Takagi-Sugeno fuzzy control structure for stabilizing an inverted pendulum via a vertical force. In the work presented by Saifizul *et al*., (2006), a Takagi-Sugeno fuzzy controller with adaptive neuro-fuzzy inference system (ANFIS) architecture has been used to affirm the stability condition of a self-erecting single inverted pendulum. Sun and Er (2004) proposed a hybrid fuzzy controller for robotic systems by combining a fuzzy gain scheduling method and a fuzzy proportional-integral-derivative (PID) controller to solve nonlinear control problems such as pole balancing and multilink robot manipulation.

For the required linear displacement of the cart wheels, sufficient torque needs to be applied at the wheels. A fuzzy controller can be designed to produce the torque using the error and change of error of the vehicle displacement. However, there is still the effect of the disruption applied to the IB with the disturbance force. As the torque produced by the fuzzy controller will not be enough for achieving the upright position of the IB, an additional torque needs to be produced to bring the rod back to the upright position using the tilt angle information as input to the fuzzy controller. This will result in a multi-input multi-output (MIMO) fuzzy controller, which will incur a huge time consuming rule-base. Therefore, for simplicity and reducing the processing time, the fuzzy controller is split into two PD-like fuzzy controllers, as shown in Figure-4, utilizing the error and the derivative of error for both the measured tilt angle of IB and linear displacement of the vehicle. This will reduce the rule-base drastically and the associated processing time. The controller outputs τ_1 and τ_2 are added into a final output as shown in Figure-4.

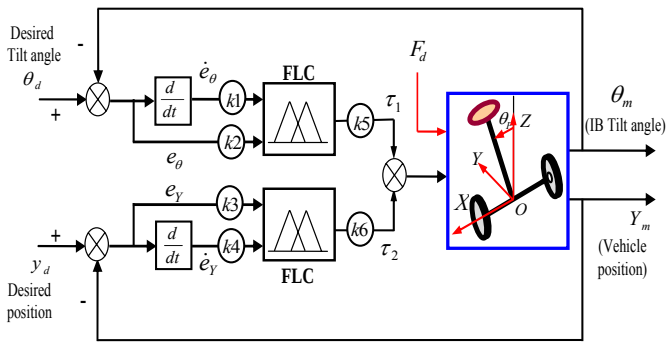

Figure-4. Schematic description of the fuzzy logic control scheme.

The control inputs are the error and the derivative of error for the two measured variables of the system Y_m and θ_m whereas the control outputs are the terminal voltages of the DC motors. As the type of motion considered in this study is linear, the two control signals from both the feedback loops are identical and hence the motor terminal voltage considered as the system input is a summation of both the voltages to the left and right wheels. The tilt angle error and its time derivative are defined as:

$$e_\theta = \theta_d - \theta_m \quad (6)$$

$$\dot{e}_\theta = \frac{d(e_\theta)}{dt} = \frac{\theta(k) - \theta(k-1)}{\Delta t} \quad (7)$$

Similarly, displacement error and its derivative are defined as:

$$e_Y = Y_d - Y_m \quad (8)$$

$$\dot{e}_Y = \frac{d(e_Y)}{dt} = \frac{Y(k) - Y(k-1)}{\Delta t} \quad (9)$$

Where θ_d is the desired tilt angle, θ_m is the measured tilt angle of IB, Y_d is the desired linear vehicle position, and Y_m is the measured vehicle position.

Five linguistic variables for the error and derivative of error, shown in Table-1, are chosen for each inputs and outputs: negative big (NB), negative small (NS), zero (Z), positive small (PS), and positive big (PB). Triangular membership functions (MFs) are chosen for each linguistic variable.

Table-1. FLC rule base.

Change of error / Error	NB	NS	Z	PS	PB
NB	**NB**	**NB**	**NB**	**NS**	Z
NS	**NB**	**NB**	**NS**	**Z**	PS
Z	**NB**	**NS**	**Z**	**PS**	PB
PS	**NS**	**Z**	**PS**	**PB**	PB
PB	Z	PS	PB	PB	PB

Triangular membership functions are chosen for inputs and outputs. The membership functions for IB angle error, derivative of IB angle error, vehicle position error, derivative of vehicle position error and voltage input are shown in Figure-5. Normalized universes of discourse are used for signals. The parameters of the two PD-like FL controllers k_1, k_2 k_3 and k_4 are selected and tuned to achieve a desired system performance. Scaling factors k_5 and k_6 are selected such that they activate the system to generate the desired output. To construct a rule base, the IB angle error, the derivative of IB angle error, the vehicle position error, the derivative of vehicle position error and

the voltage input are partitioned into five primary fuzzy sets.

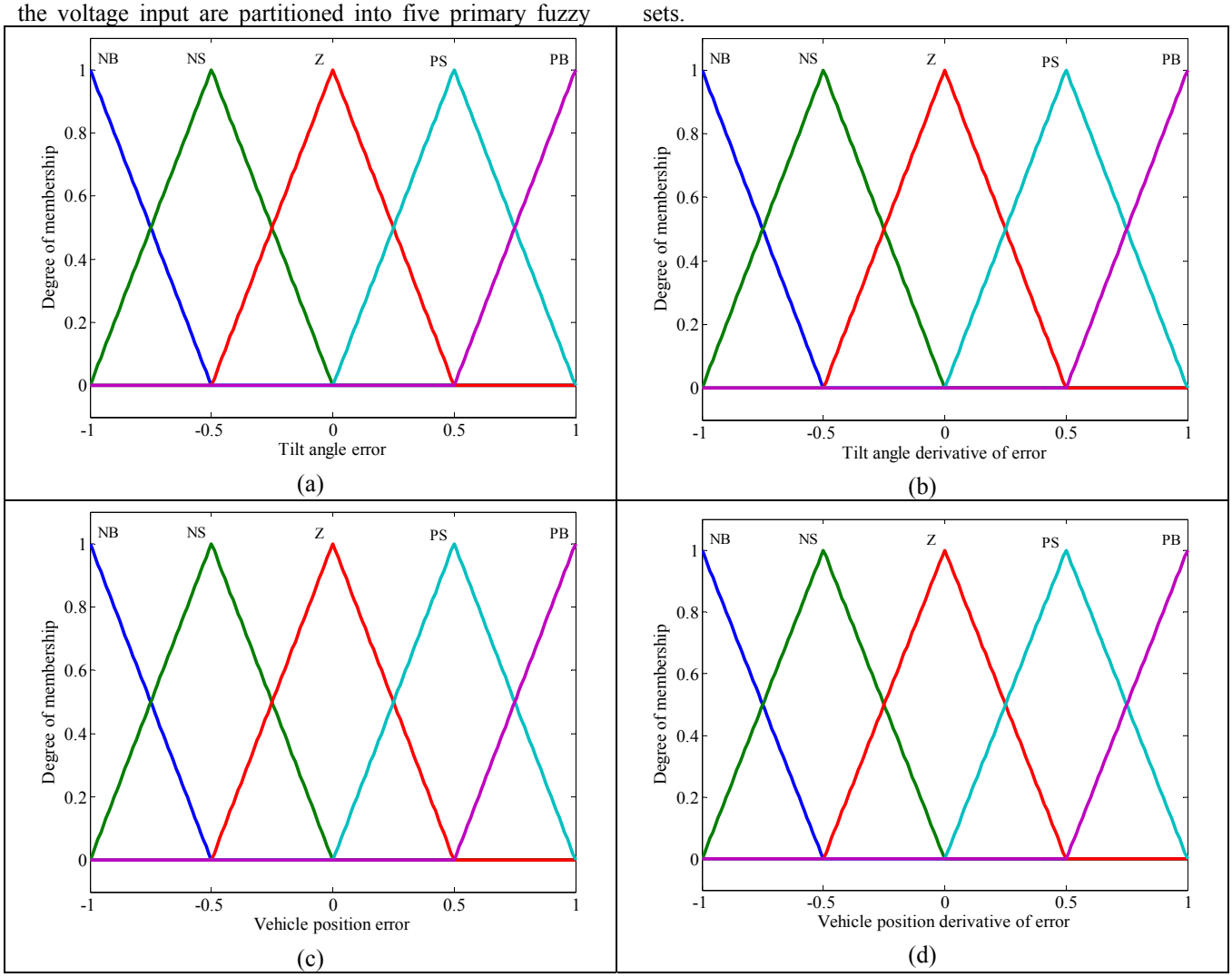

Figure-5. Membership functions of the fuzzy logic controllers.

4. SIMULATION AND ANALYSIS OF RESULTS

Simulations were carried out on the system using the numerical parameters describing the system features as listed in Tables 2 and 3.

Table-2. DC motor technical specifications.

Parameter	Description	Units
$R = 3$	Nominal terminal resistance	*Ohms*
$L = 0$	Rotor inductance	*H*
$K_e = 0.0061$	Back EMF constant	Vs/rad
$V_e = 0$	Back EMF voltage	*Volts*
$I_r = 0$	Rotor inertia	kgm^2

Table-3. Two-wheeled inverted pendulum mechanical properties.

Parameter	Description	Units
$R_w = 0.1$	Wheel radius	*m*
$M_w = 1$	Wheel mass	*kg*
$M_p = 5$	Pendulum mass	*kg*
$M = 10$	Payload	*kg*
$M_a = 0.7$	Wheels connecting axle mass	*kg*
$M_a = 0.5$	Motor mass	*kg*
$M_{gearbox} = 0.35$	Reduction gear box mass	*kg*
$l = 0.25$	Length to the pendulum centre of mass centre of mass	*m*

The simulations were conducted to highlight the way the vehicle will behave with the effect of changing

the values of different variables and the control effort required to accomplish the required task. Investigation is carried out with the effect of the following variables:

- The level of the applied disturbance force; force amplitude
- The duration of the disturbance force; force duration
- The position of disturbance force,
- Position and speed of the payload.
- IB length.

4.1 Payload static behaviour

Let the payload, M be located at a distance Q from the IB origin O, as shown in Figure-A2 (Appendix), where Q can be expressed as a factor y multiplied by the rod half length l as:

$$Q = y\,l \tag{10}$$

Where $0 \le y \le 2$ according to the position of the payload M from the origin of the IB. Changing the payload position will affect both the overall moment of inertia, I_g and the location of the global centre of mass of the IB, L_g. The overall moment of inertia of the IB is affected and modified as:

$$I_g = \frac{M_p(2l)^2}{12} + M_p\left(L_g - l\right)^2 + M\left(Q - L_g\right)^2 \tag{11}$$

The location of the global centre of mass of the IB will be affected as:

$$L_g = \frac{\left(M_p l + QM\right)}{\left(M_p + M\right)} \tag{12}$$

4.1.1 Effect of different disturbance levels

The effect of changing the level of the applied disturbance force is considered in this section. Four levels of disturbance amplitudes including zero are considered to test the validity of the developed controller in coping with external disturbances. The simulations are carried out by considering the disturbance force applied at different positions on the IB of the vehicle. Such assumptions may be useful in applications such as extended height of crane arms if subjected to sudden external forces through their stems especially during motion.

Figures 6 to 11 show the system performance with the disturbance force applied at the upper end, mid-span and lower end of the IB. It can be noted from Figures 6(a), 7(a), 8(a), 9(a), 10(a) and 11(a) that the higher the level of the disturbance force the longer the fluctuation of the rod angle from the upright position. It can also be noted that the closer the location of the applied disturbance force to the IB origin the harder it is to balance the system as it takes the control system a long time to bring the rod to the target position.

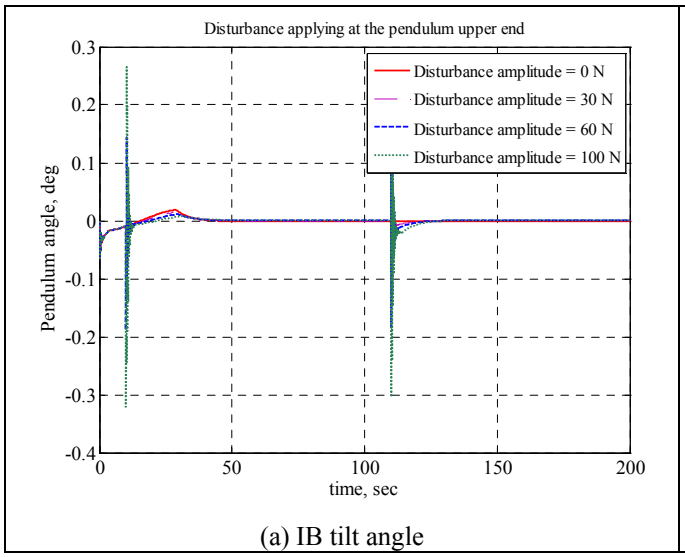

(a) IB tilt angle

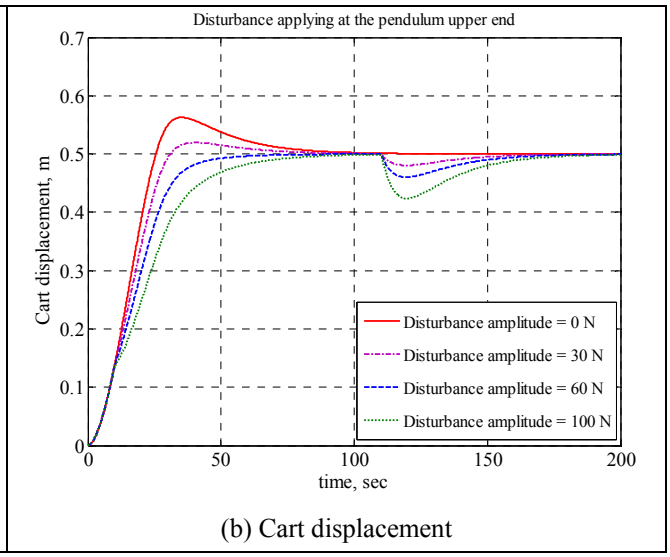

(b) Cart displacement

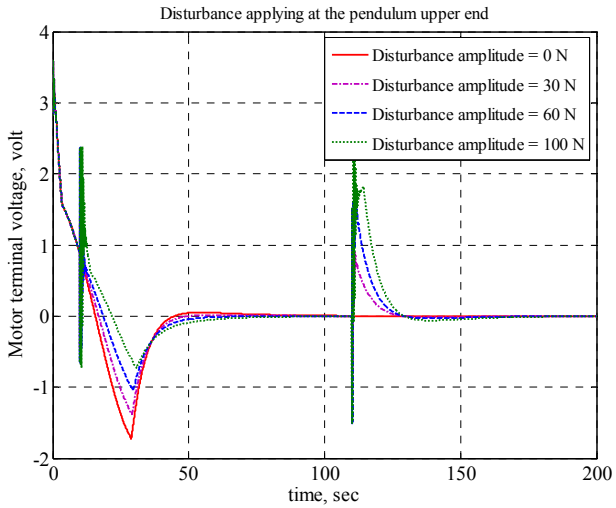

(c) Motor terminal voltage

Figure-6. System performance and control signal (Upper end disturbance application); *y = 2*, PD control.

The cart linear displacement is presented in Figures 6(b), 7(b), 8(b), 9(b), 10(b) and 11(b). It is noted that increasing the level of the applied disturbance tends to decrease the cart overshoot beyond the specified limit. That is because the amount of the applied force acts as a drag force for the cart and slows the cart which in turn increases the rise time of the system response. This phenomenon is clearly repeated when the force is reapplied on the system. The lower the level of the disturbance forces the faster the cart in achieving the desired position.

Changing the level of the disturbance force also affected the control effort, as clearly shown in Figures 6(c), 7(c), 8(c), 9(d), 10(d) and 11(d). Higher levels of the applied force tended to increase the time the control signal takes to settle down. The location of the disturbance force also greatly affected the control behaviour. The closer the position of the force to the rod origin the more the control effort fluctuation and the higher the control effort at the time of applying the force.

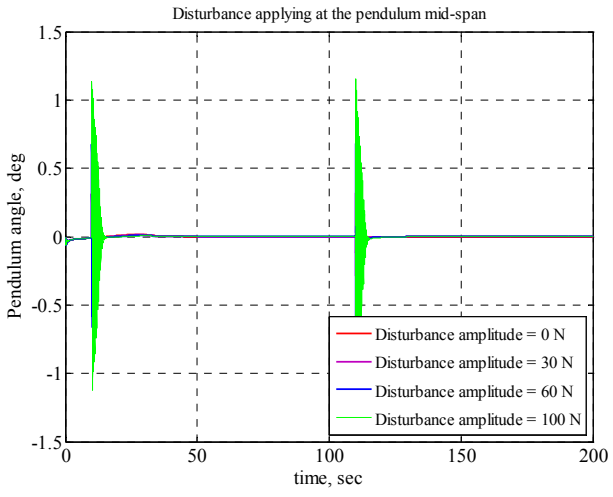

(a) IB tilt angle

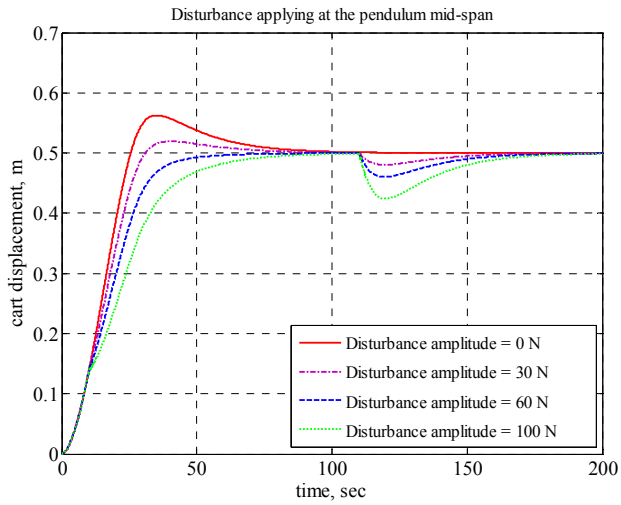

(b) Cart displacement

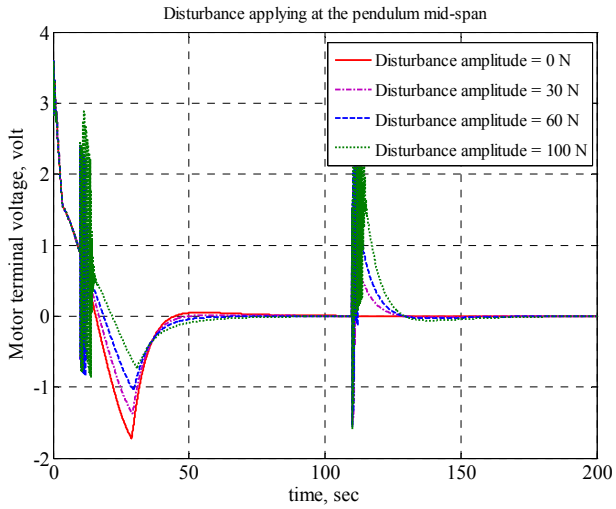

(c) Motor terminal voltage

Figure-7. System performance and control signal (Mid-span disturbance application); $y = 1$, PD control.

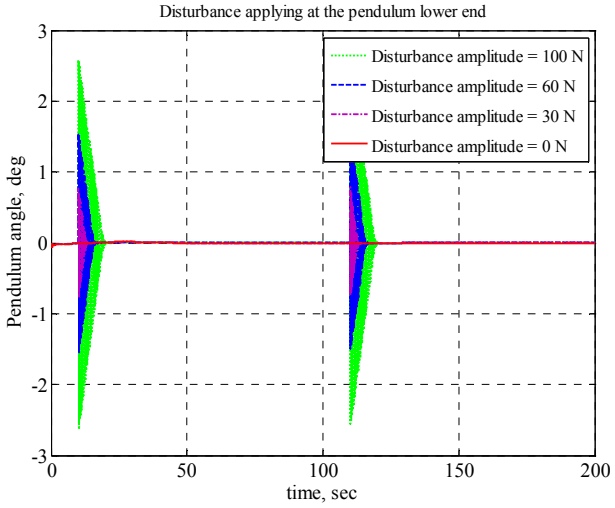

(a) IB tilt angle

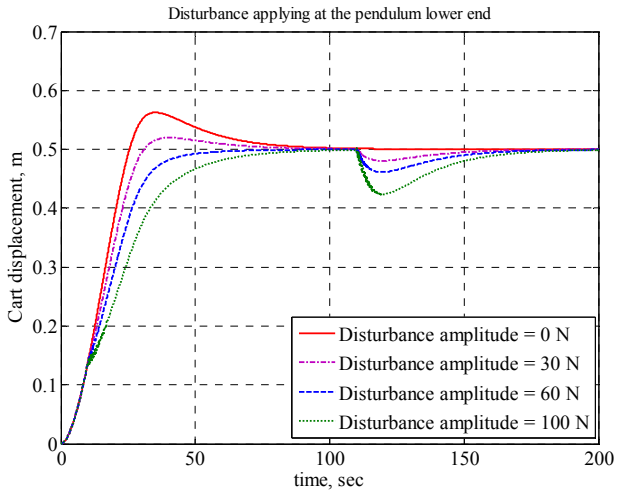

(b) Cart displacement

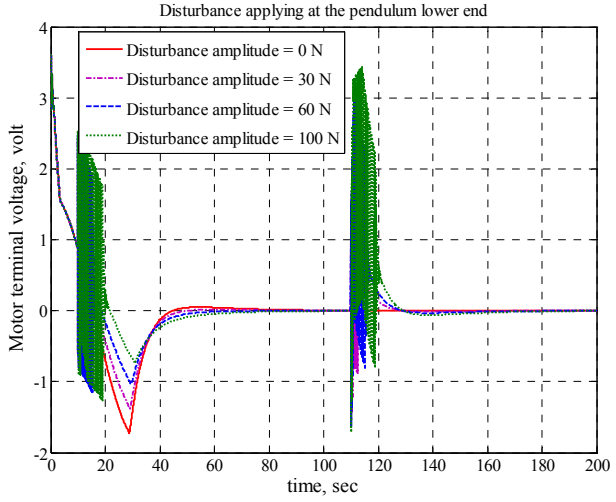

(c) Motor terminal voltage

Figure-8. System performance and control signal (Lower end disturbance application); $y = 0$, PD control.

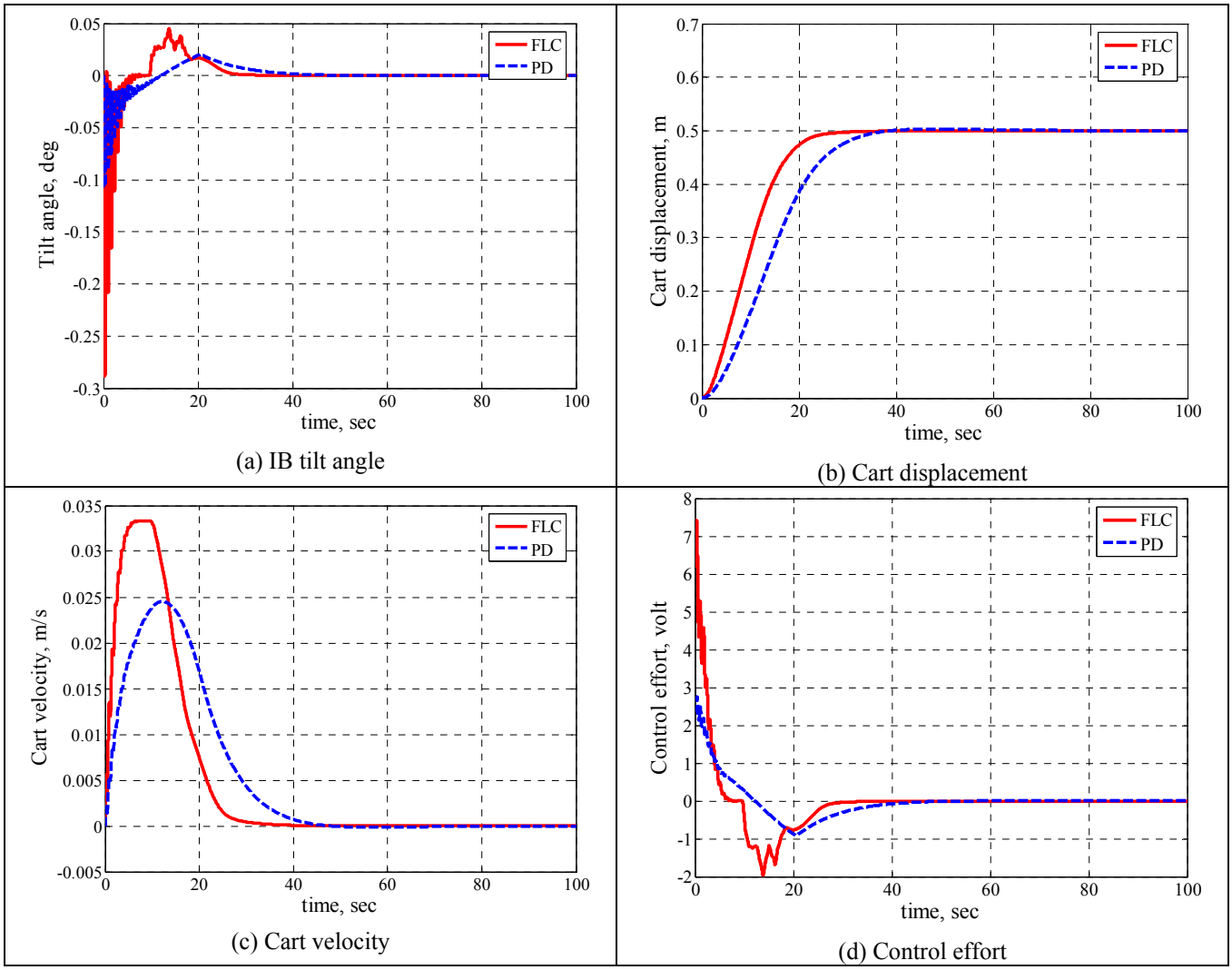

Figure-9. Simulation results (*F = 0 N*).

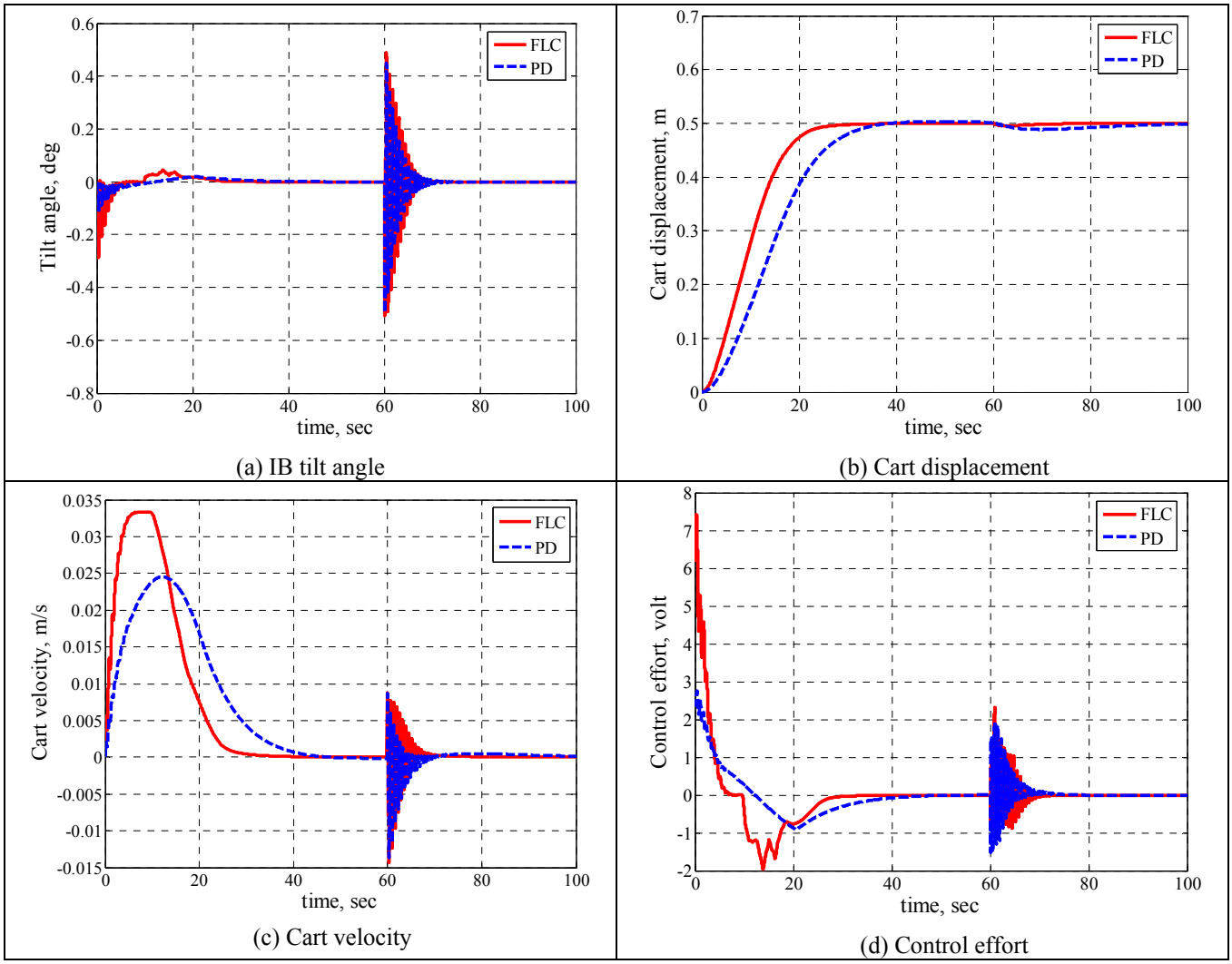

Figure-10. Simulation results (F = 30 N, t = 0.1 sec, Q =50cm).

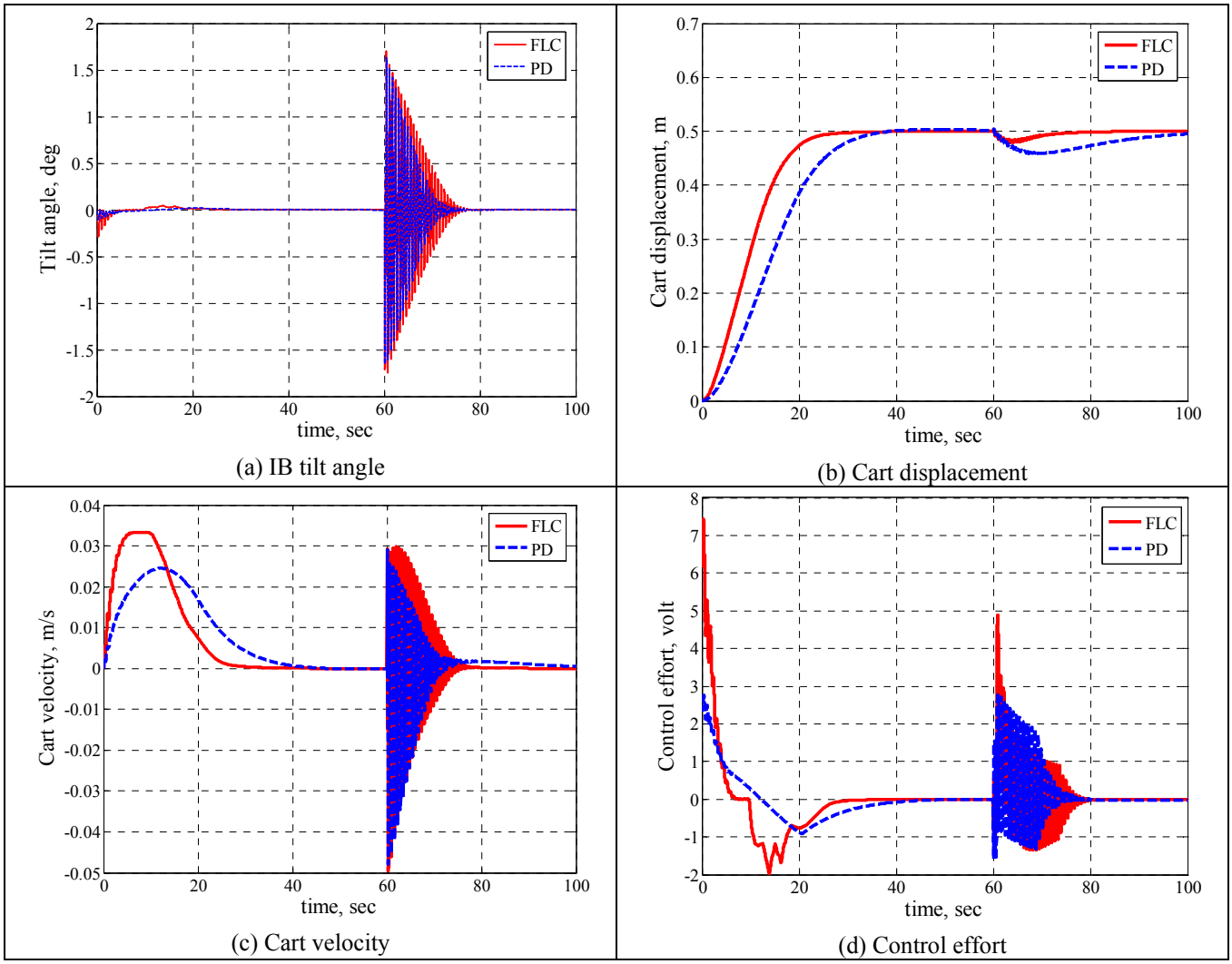

Figure-11. Simulation results (F = 100 N, t = 0.1 sec, Q =50cm).

4.1.2 Effect of disturbance duration

The duration of applying such disturbances is another variable of interest. Four different durations of the disturbance force are used to estimate the safe limits beyond which the developed controller will not be able to cope.

Figures 12(a), 13(a) and 14(a) show the IB tilt angle, with different duty cycles of disturbance force of 100 N and 30 N. It is noted that the overshoot in the IB tilt angle increased as the period of the force was increased, and the controller still coped well with such higher periods of time especially for the pendulum tilt angle. The system could recover faster to the desired position with shorter duty cycles of the force.

For the cart linear displacement, as described in Figures 12(b), 13(b) and 14(b) the situation was not as good as for the tilt angle; increasing the duty cycle of the force made the system slower in achieving the target and increased the rise time and decreased the cart overshoot. But for shorter duty cycles, the overshoot tended to be higher which is a characteristic of such impulse disturbance force but accelerated the system behaviour to reach the desired position.

The control effort is presented in Figures 12(c), 13(d) and 14(d). It is noted that the longer the disturbance duty cycle the higher the control effort required and the longer the time for the control signal to settle down.

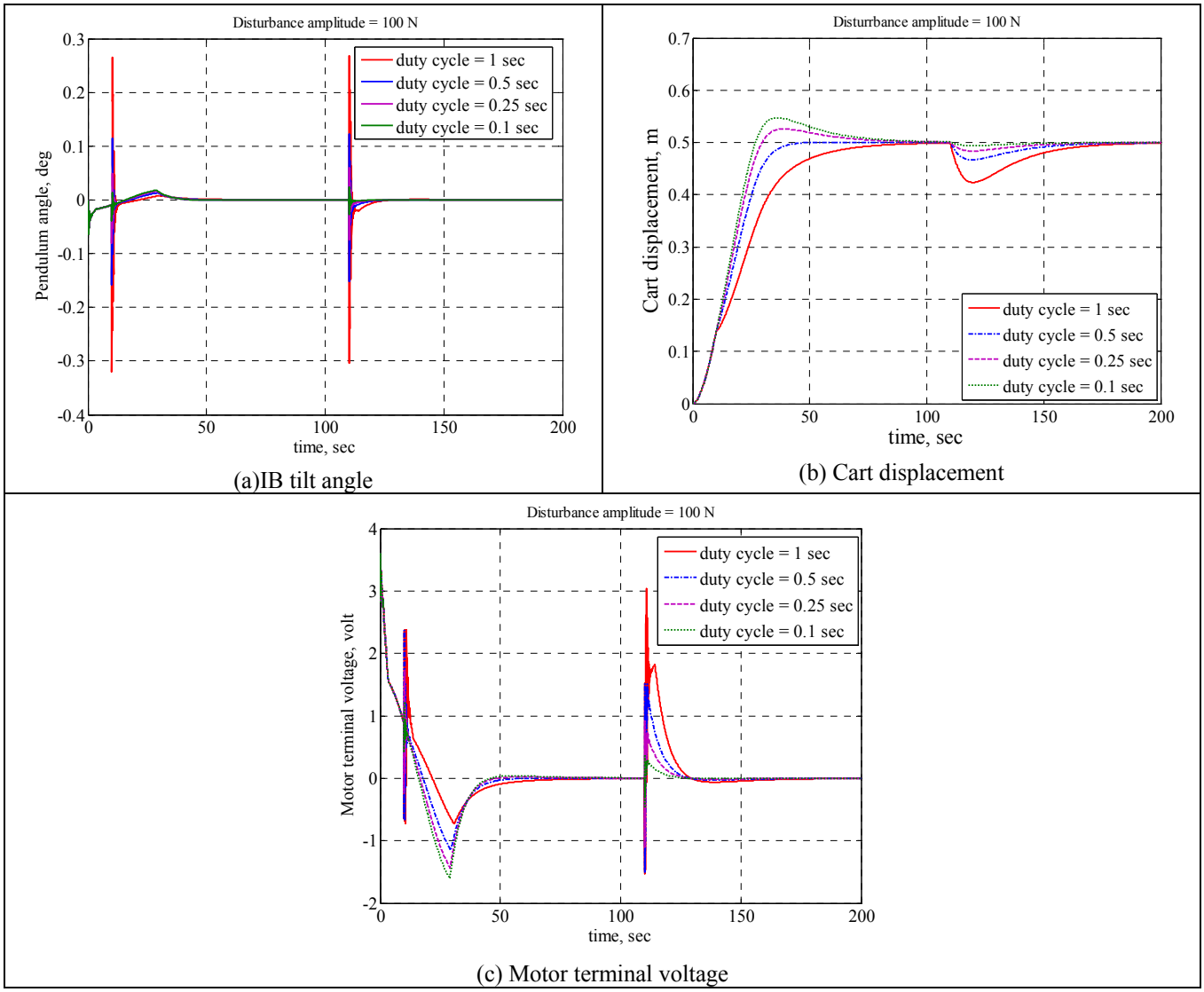

Figure-12. System performance and control signal (Different disturbance duty cycles), PD control.

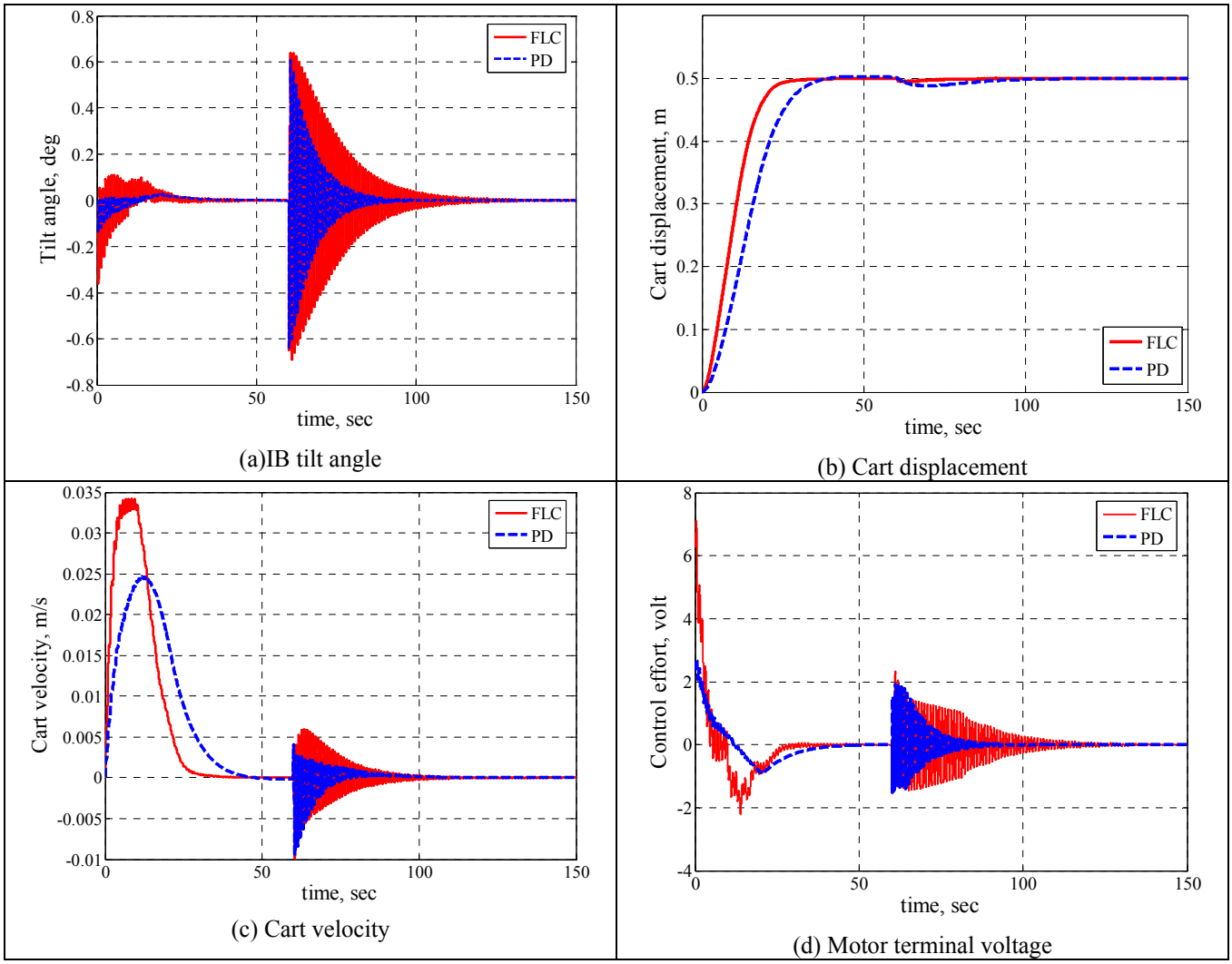

Figure-13. Simulation results (F = 30 N, t = 0.1 sec, Q =15cm).

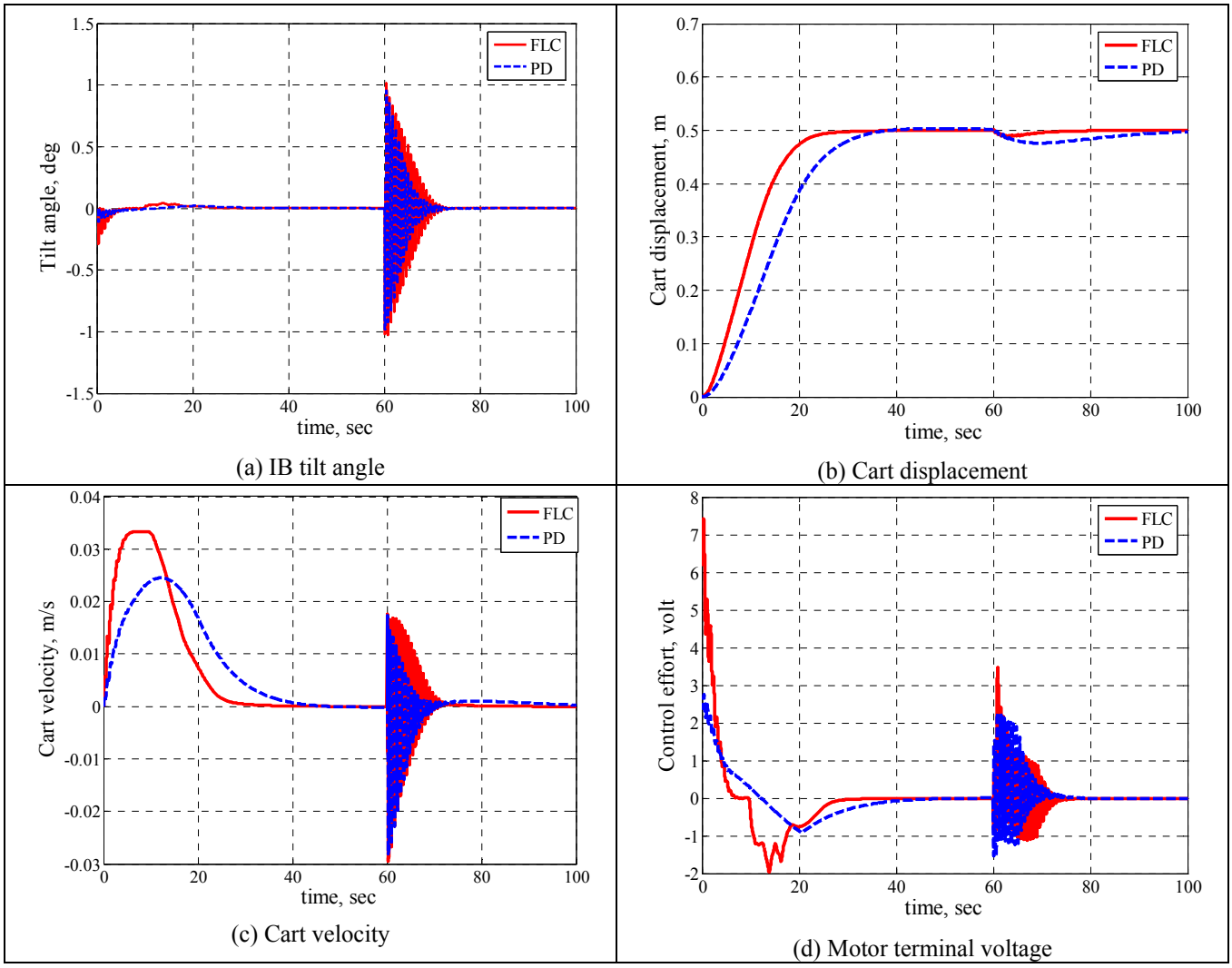

Figure-14. Simulation results (F = 30 N, t = 0.2 sec, Q =15cm).

4.1.3 Effect of payload position

The third variable of interest is the location of the payload attached to the IB. The system behaviour including the IB tilt angle and the cart linear displacement are presented and the control effort required for three different locations of the payload. The load is positioned at upper, mid-span and the lower end of the IB. Changing the location of the load mainly affects the location of the global centre of mass and the whole moment of inertia of the pendulum as presented earlier.

Three different levels of the disturbance force are implemented here with the assumption of the force at the upper end of the rod. Figures 15 to 18 show the system performance with different load positions and disturbance forces of 30 *N*, 100 *N* and 0 *N* respectively.

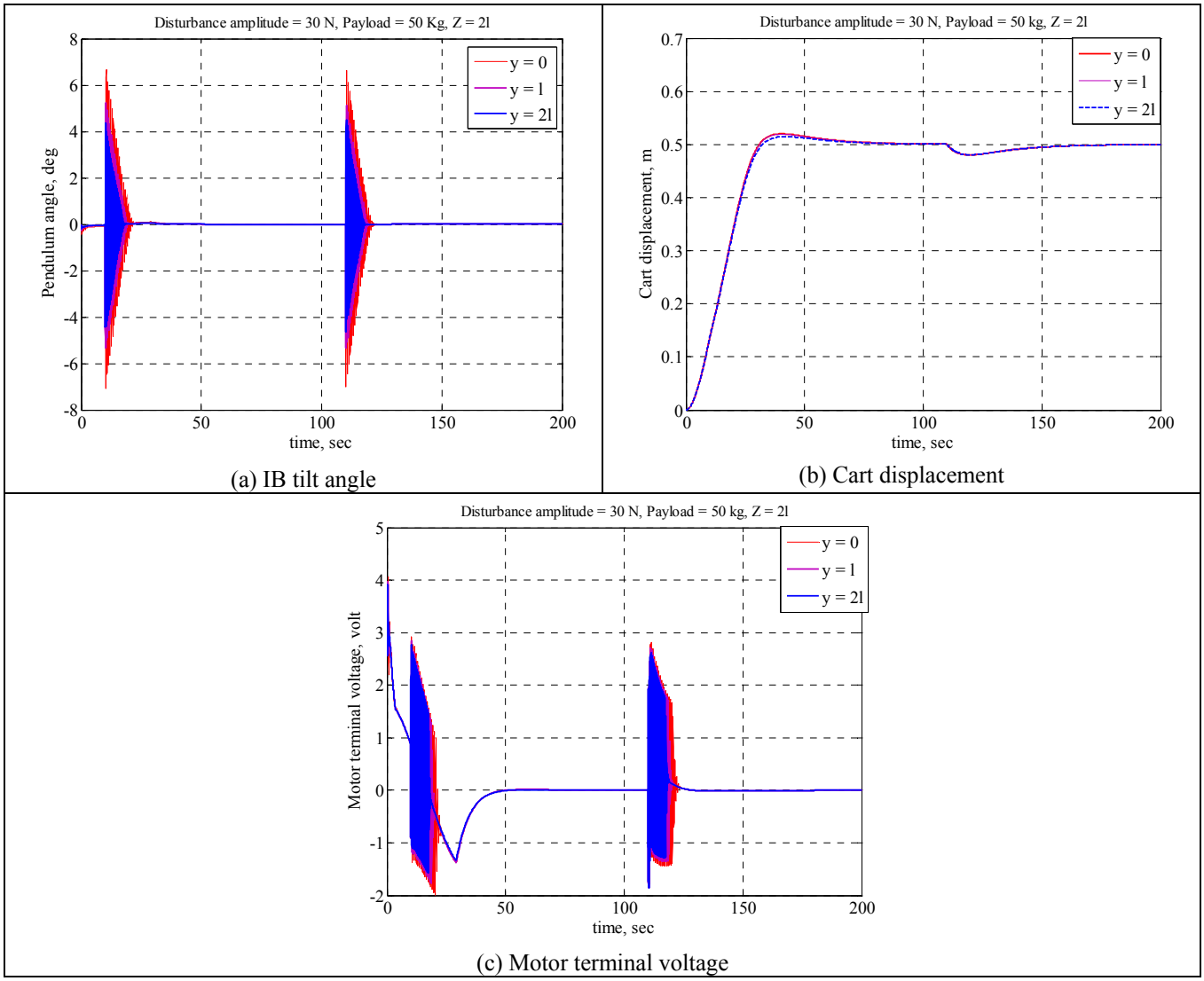

Figure-15. System performance and control signal ($F = 30\ N$), PD control.

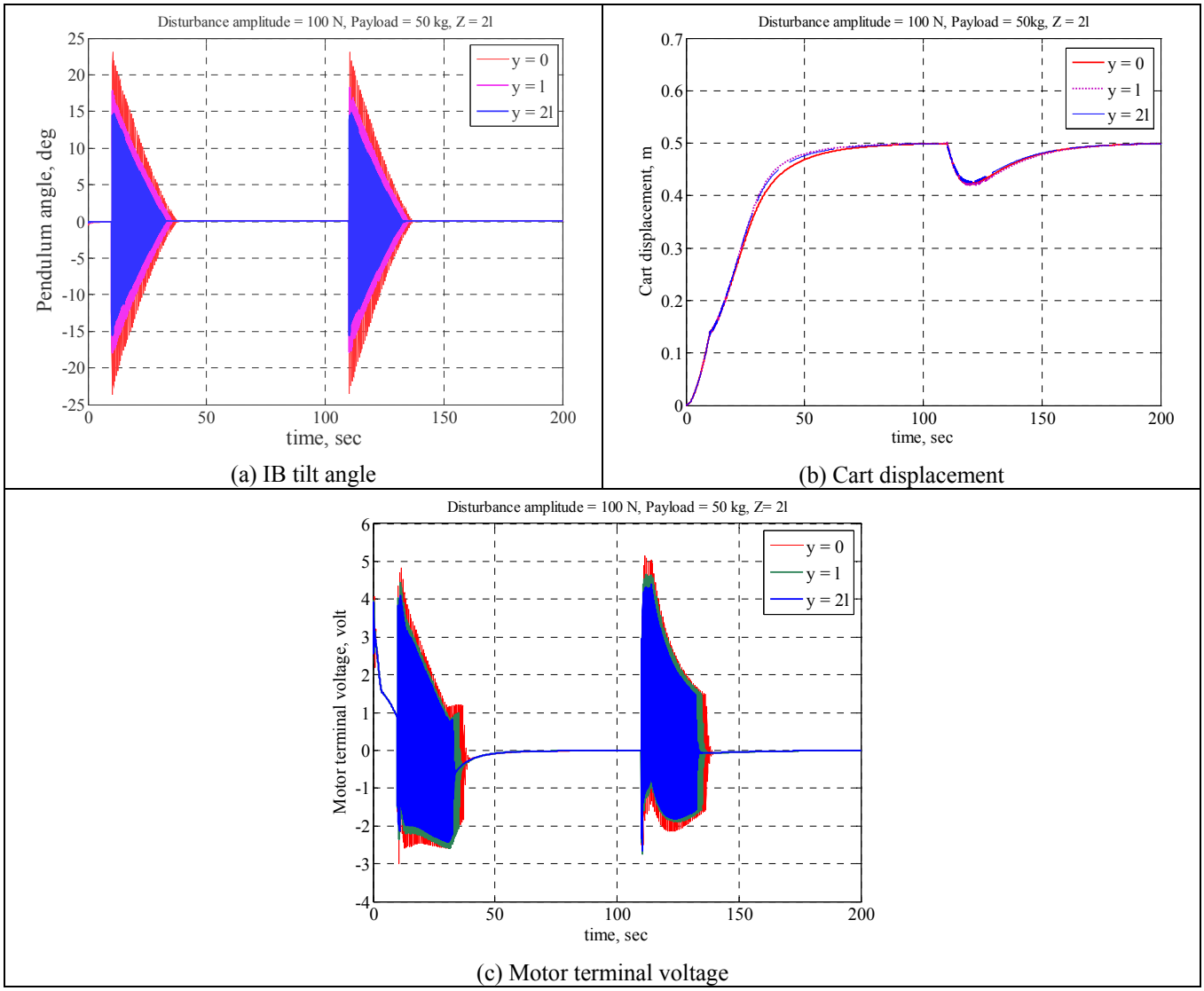

Figure-16. System performance and control signal ($F = 100\ N$), PD control.

It is noted in Figures 15(a), 16(a), 17(a) and 18(a) that the closer the payload to the IB origin the harder the balancing in the upright position. More fluctuations of the rod occur as the load is closer to the origin. This phenomenon is similar to the system behaviour for the case of applying the disturbance force at the lower end of the rod as previously described in Figure-13. Therefore, this means that the harder it is to balance the IB when either the force is applied at lower positions of the rod or the payload is closer to the origin. Hence, the worst and hardest case of balancing is more likely to happen when the payload and disturbance force are both close to the IB origin.

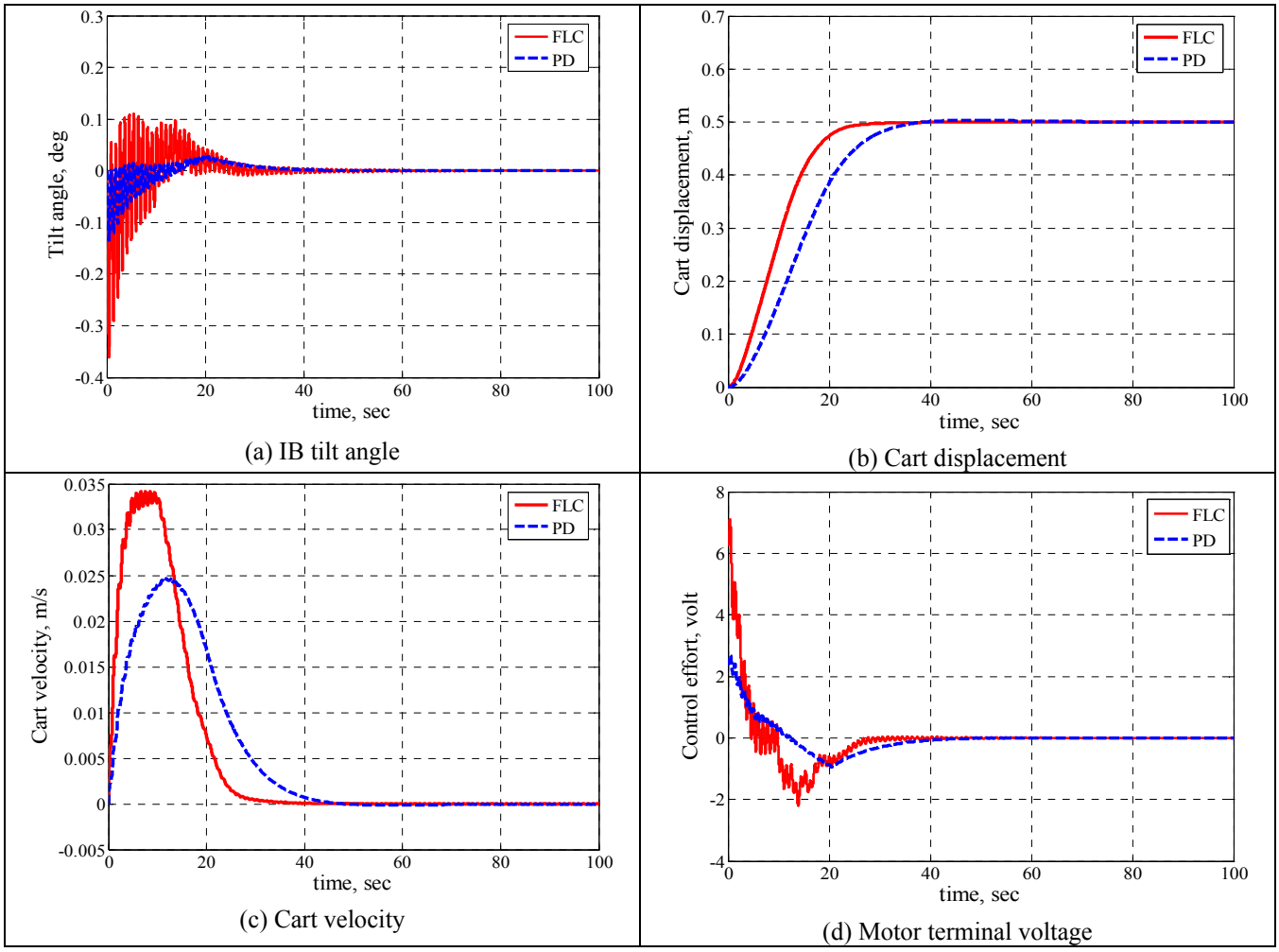

Figure-17. Simulation results (*F = 0 N, Q =15cm*).

Changing the payload position in the previous manner did not affect the cart linear displacement significantly as noted in Figures 15(b), 16(b), 17(b) and 18(b). This is still not expected to happen for longer pendulum rods. However, the effect was more due to the value of the disturbance force applied on the rod. The control effort appears to have more fluctuations when the payload was closer to the origin as noted in Figures 15(c), 16(c), 17(d) and 18(d).

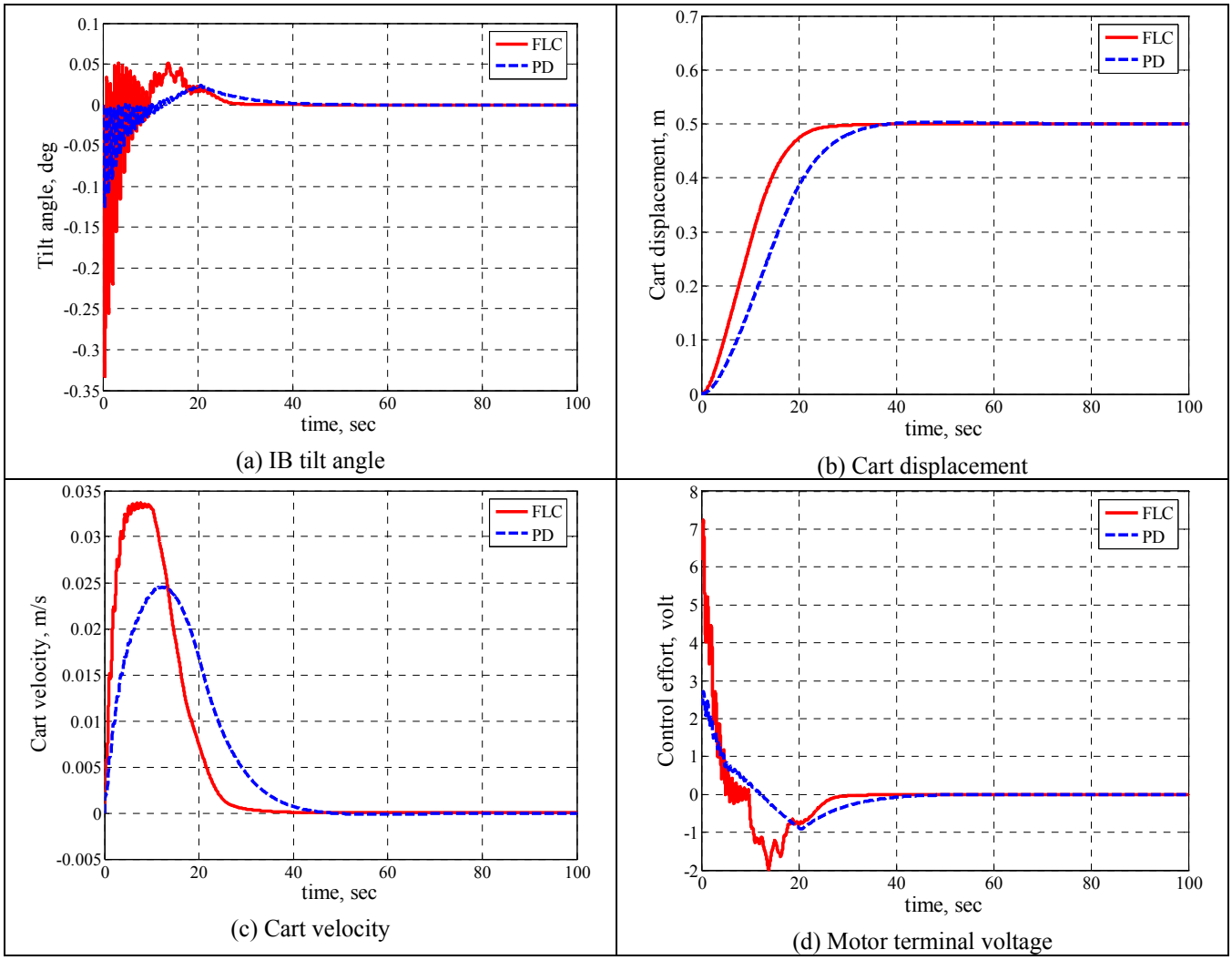

Figure-18. Simulation results (*F = 0 N, Q =25cm*).

4.2. Virtual dynamic payload motion

For dynamic motion of the payload, the payload M is assumed to move virtually up and down with a simple harmonic motion expressed as:

$$y = Amp\sin(freq*t + phase) + bias \quad (13)$$

Select $Amp = 1$, $freq = f$, $phase = 0$, $bias = 1$

Then the motion of the payload can be described as:

$$Q = l\sin(f*t) + 1 \quad (14)$$

$$\dot{Q} = lfc\cos(f*t) \quad (15)$$

and

$$\ddot{Q} = -lf^2\sin(f*t) \quad (16)$$

Where Q, $\dot{Q}$ and $\ddot{Q}$ are the linear displacement, velocity and acceleration of the payload

4.2.1 Motion of the payload and the centre of mass

The linear motion executed by the payload along the IB is described in Figures 19 and 20. The payload is assumed to move up and down along the IB as a simple harmonic motion.

As the payload is moving in this way, the location of the COM of the IB will keep changing as noted in Figures 19(b) and 20(b). The payload is assumed initially at the mid-span of the IB, then moving up till the upper end and then down to the lower end of the rod and continuing up and down until the end of the simulation.

As noted in Figure-20(a), the COM of the IB will never reach the extreme ends of the IB unless the mass of the rod is assumed negligible compared to the payload. Figure-19(b) shows the velocity of the payload along the IB. The payload speed is changing dramatically at the start of the simulation; such behaviour is not desirable in the system performance as the payload acceleration will increase and that in turn leads to a jerky motion. Such situation is dominant for higher changes of velocity in a finite time.

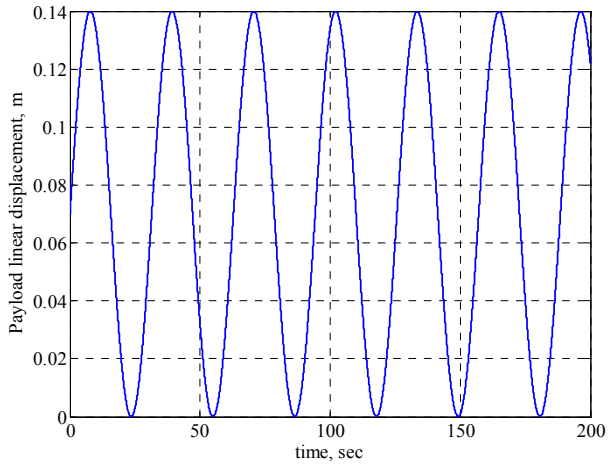

(a) Payload displacement

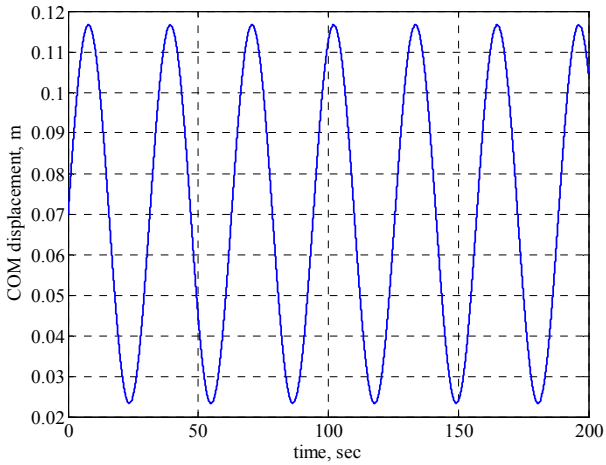

(a) COM displacement

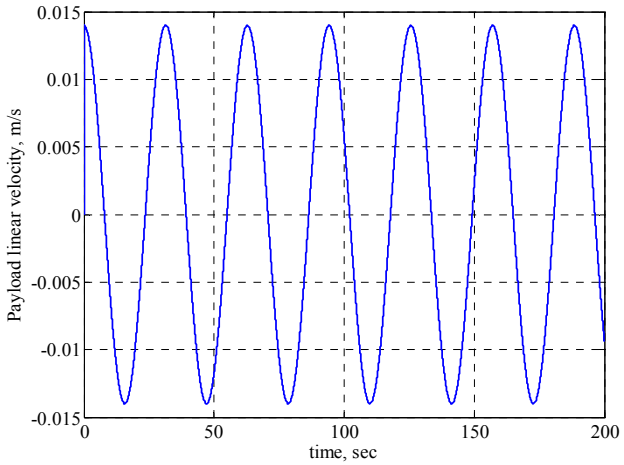

(b) Payload velocity

Figure-19. Payload linear motion (*Frequency* = 0.1 *Hz).*

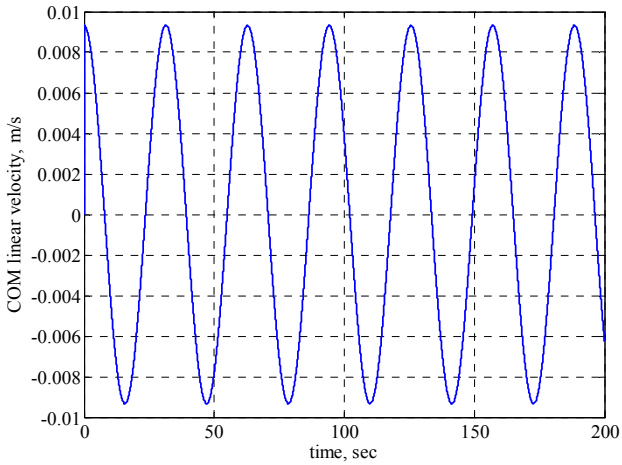

(b) COM velocity

Figure-20. *COM* linear motion (Frequency = 0.1 Hz).

The speed of the COM position, as presented in Figure-20(b), is around half the value of the payload speed. This will be different for different values of payload and rod mass.

4.2.2 Effect of different disturbance levels

The effect of changing the level of the applied disturbance force is considered in this section. Four levels of disturbance amplitudes are considered from 10 N to 150 N in order to test the performance and robustness of the developed controller such different impact levels. The simulation is carried out by considering the disturbance force applied at the upper end of the IB of the vehicle.

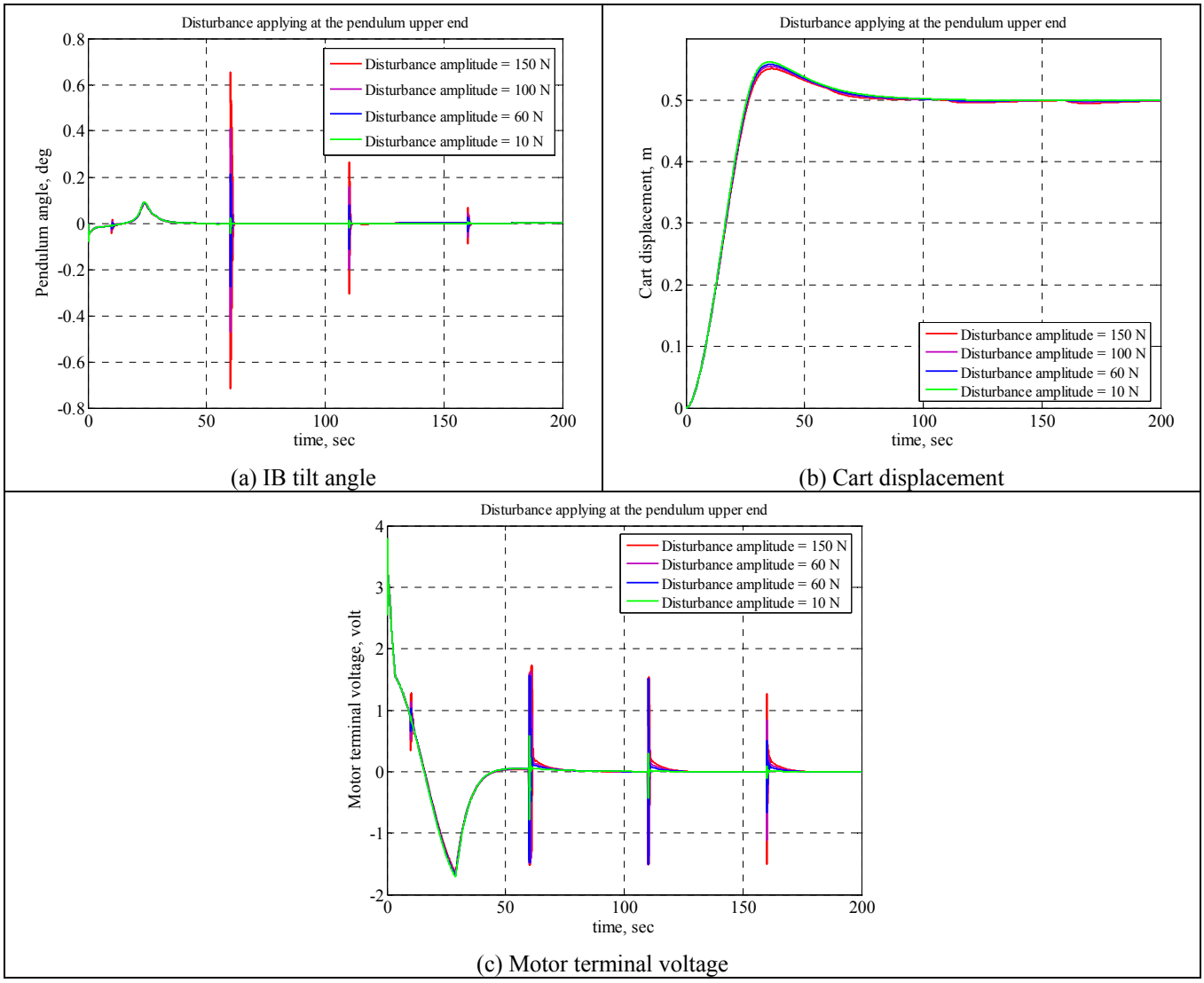

Figure-21. System performance and control signal (Different disturbance levels), PD control.

It can be noted from Figures 21(a), 22(a) and 23(a) that the higher the level of the disturbance force the higher the fluctuation of the rod angle from the upright position and the longer it takes the IB to balance at the upright position.

The cart linear displacement is presented in Figures 21(b), 22(b) and 23(b). It is noted that increasing the level of the applied disturbance tends to decrease the cart overshoot beyond the specified limit. This is because the amount of the applied force acts as a drag for the cart and slows the cart which in turn increases the rise-time of the system response. This phenomenon is clearly repeated when the force is reapplied on the system. It can also be noted that the lower the level of the disturbance force, the faster the cart in achieving the desired position.

Changing the level of the disturbance force also affected the behaviour of the controller, which is clearly presented in Figures 21(c), 22(d) and 23(d). Higher levels of the applied force tended to increase the time the control signal takes to settle down and also required a lot of control effort.

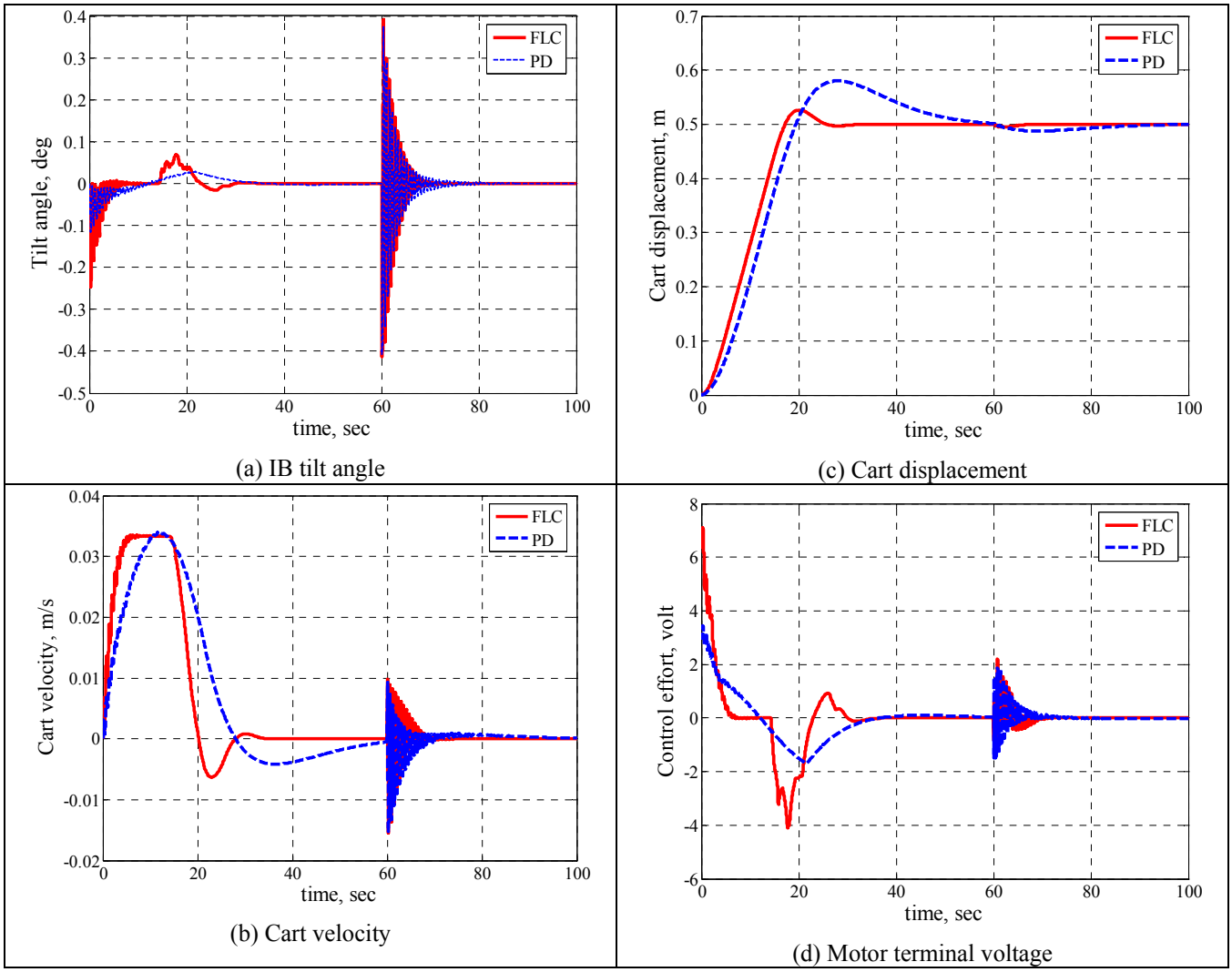

Figure-22. Simulation results (F = 30 N, t = 0.1 sec, f = 0.1 Hz).

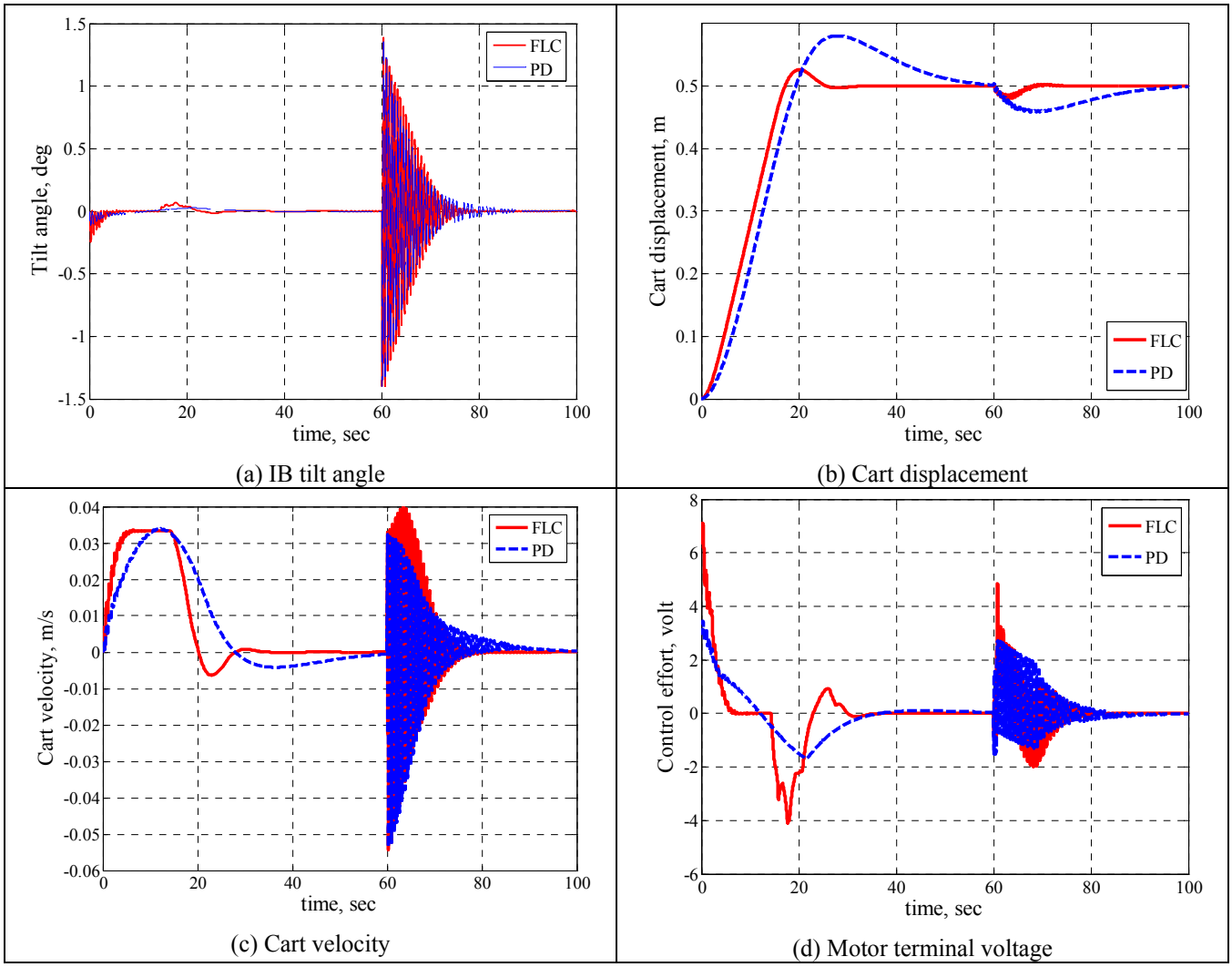

Figure-23. Simulation results (F = 100 N, t = 0.1 sec, f = 0.1 Hz).

4.2.4 Effect of disturbance duration

The duration of applying such disturbances is another variable of interest. Four different periods of the disturbance force are used to estimate safe limits beyond which the developed controller will not be able to cope with. Two different levels of disturbance force are used to test the validity of the developed control algorithm at different disturbance duty cycles.

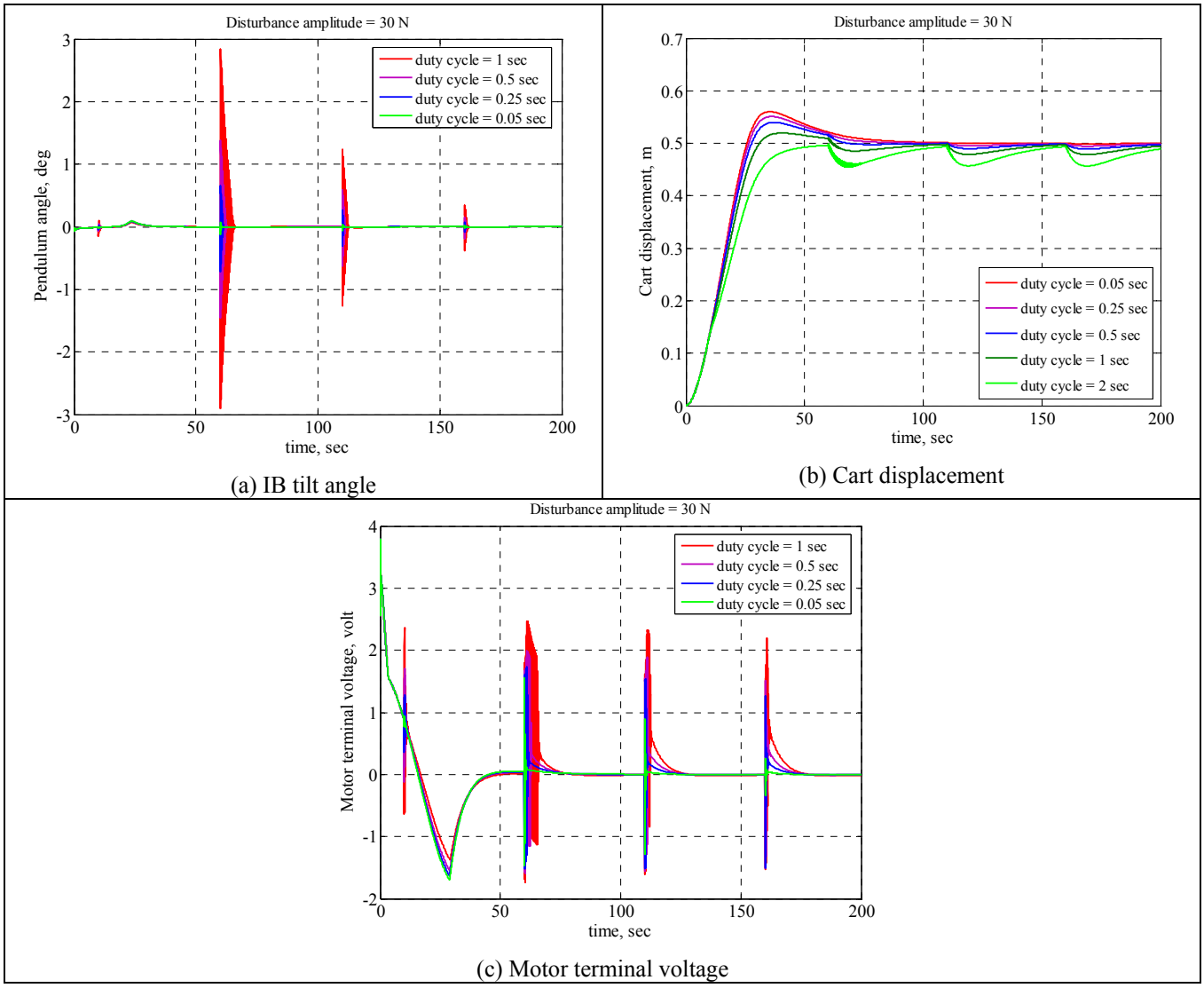

(a) IB tilt angle

(b) Cart displacement

(c) Motor terminal voltage

Figure-24. System performance and control signal (Disturbance amplitude = 30 *N*), PD control.

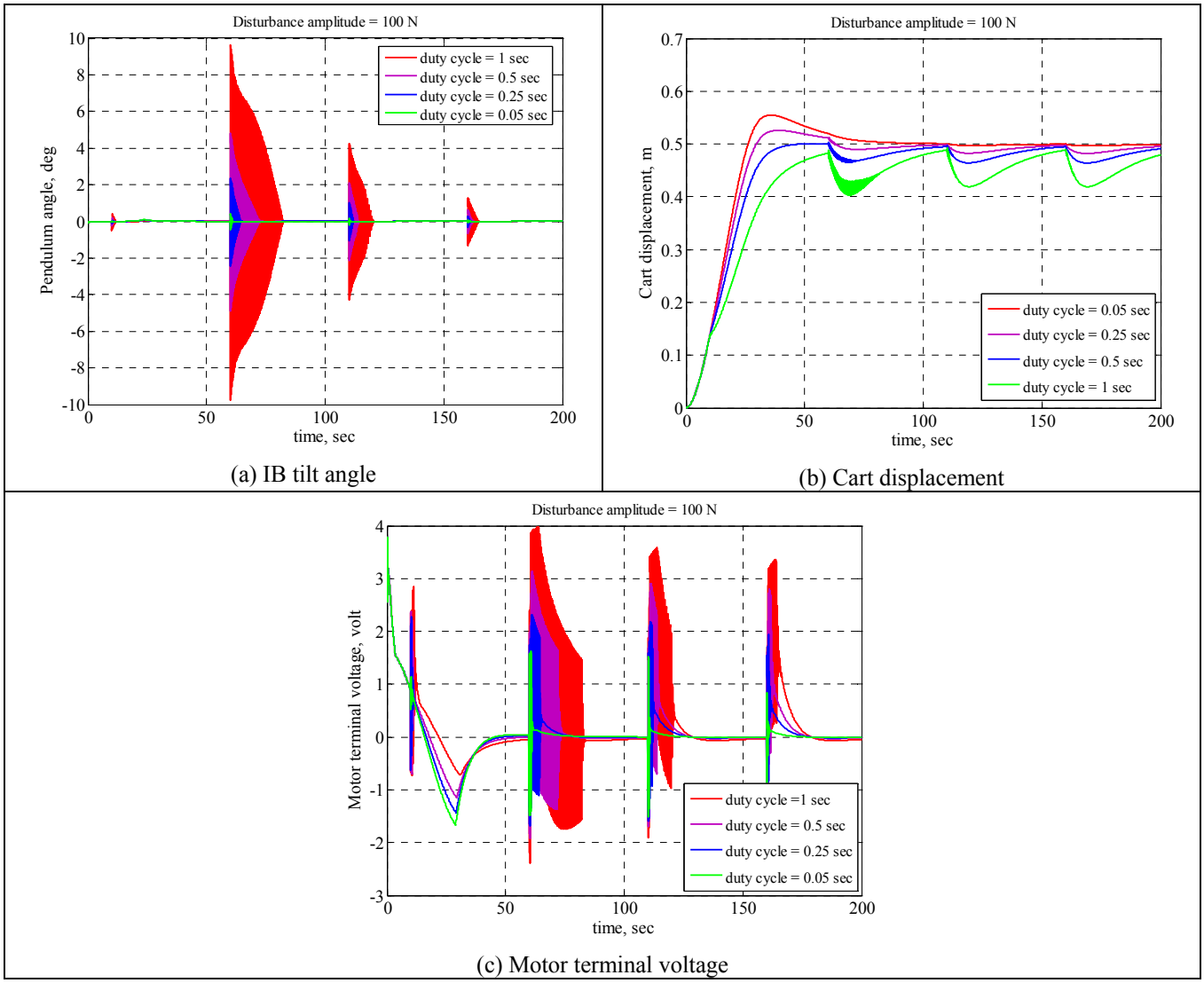

Figure-25. System performance and control signal (Disturbance amplitude = 100 *N*), PD control.

From Figures 24(a), and 25(a), it is noted that the amount of overshoot in the IB tilt angle increases as the period of the force is increased. Also the system can recover faster to the desired position with lower values of the duty cycle of the force. The controller still copes well with such higher periods of time especially for the pendulum tilt angle. The amount of tilt angle overshoot and the duration of fluctuations until the system settles down are proportional to the level of the disturbance force applied to the system.

For the cart linear displacement, as described in Figures 24(b), and 25(b), the situation is not as good as for the tilt angle, as increasing the force duty cycle made the system slower in achieving the target, increased the rise-time and decreased the cart overshoot. However, for lower values of time, the overshoot tended to be higher, which is a characteristic of such impulse disturbance force, but accelerated the system to reach the desired position. It can also be noted that the effect of repeating the disturbance force is more dominant at higher levels of disturbance force than the situations at the lower levels. The reason behind that is the accumulation of errors in the cart position.

The control effort is presented in Figures 24(c), and 25(c). It is noted that the longer the disturbance duty cycle the higher the control effort required and the longer the time for the control signal to settle down.

The same conclusions will hold for the results in Figures 22 and 26, based on the implementation of PD-like fuzzy control technique.

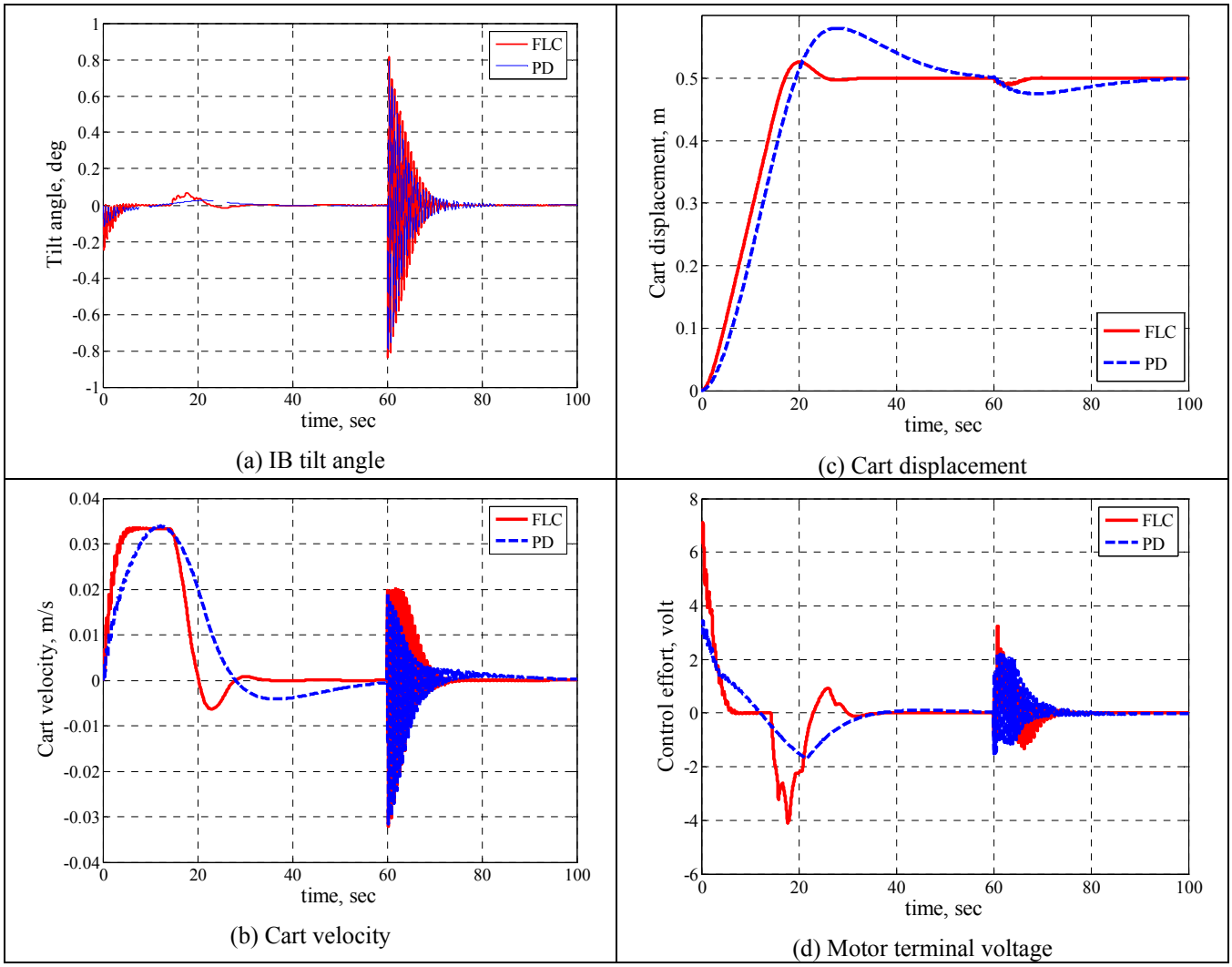

Figure-26. Simulation results (F = 30 N, t = 0.2 sec, f = 0.1 Hz).

4.2.5 Effect of payload speed

Simulations were carried out with the effect of changing the payload speed along the IB. The speed of the payload can be changed if the frequency of simple harmonic motion of the payload is changed. Four different levels of such frequency are implemented to investigate the effect of speed change on the performance of the system and the ability of the controller to overcome the results which may arise in such cases.

The linear motion executed by the payload along the IB is described in Figures 27 (a) and 28(a). The payload is assumed to move up and down along the IB in a simple harmonic motion. As the frequency of the payload motion increases 10 times from 0.1Hz to 1Hz the speed of the payload will increase around 6 times based on the formula in equation (15).

As the payload is moving in this way, the location of the COM of the IB will keep changing as noted in Figures 27(b) and 28(b). The payload is assumed initially at the mid-span of the IB, then moving upward till the upper end and then down to the lower end of the rod and continuing up and down until the end of the simulation.

As noted in Figures 27(b) and 28(b), the COM of the IB will never reach the extreme ends of the payload unless the mass of the rod is assumed negligible compared to the payload.

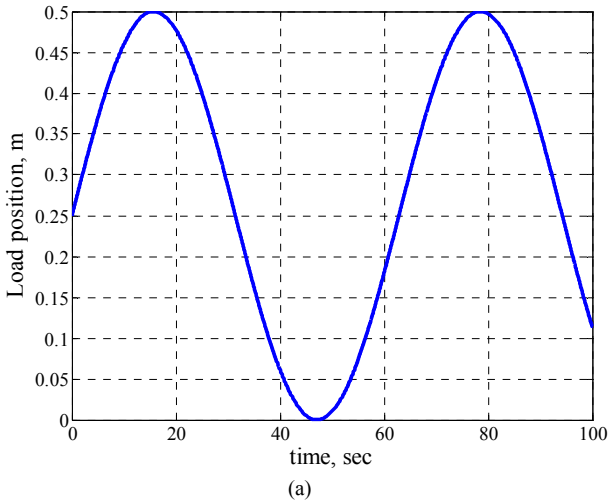

(a)

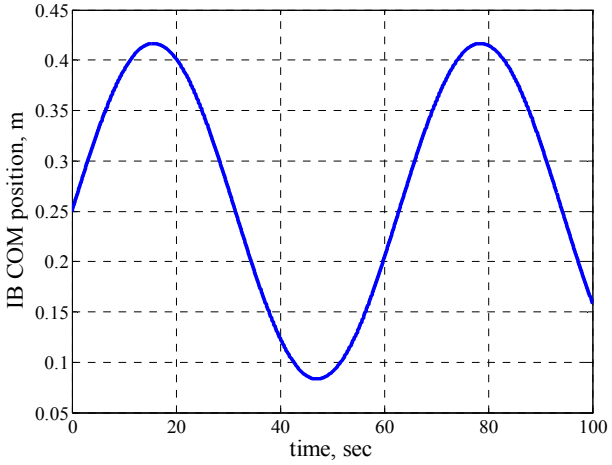

(b)

Figure-27. Payload and COM motion (Motion frequency, f = 0.1 Hz).

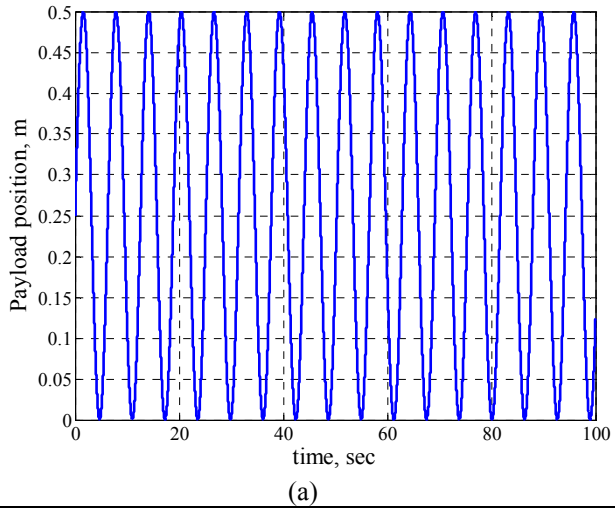

(a)

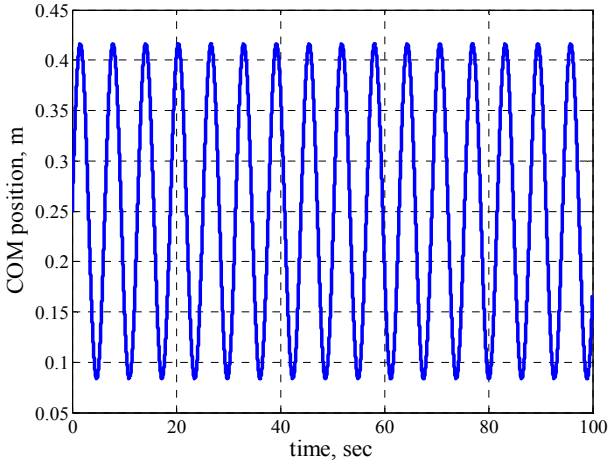

(b)

Figure-28. Payload and COM motion (Motion frequency, f = 1 Hz).

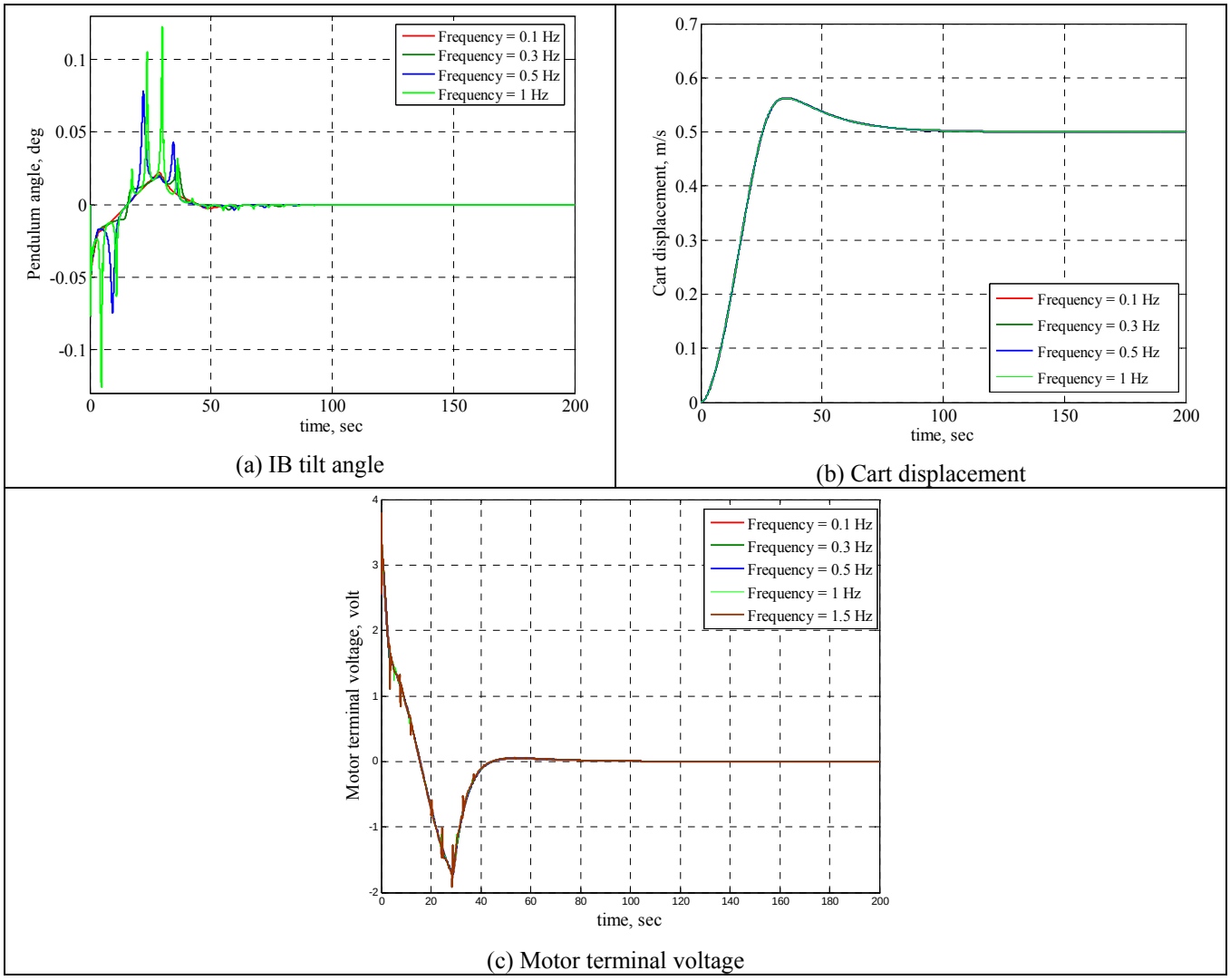

Figure-29. System performance and control signal (different payload speeds), PD control

The IB tilt angle is shown in Figures 29(a), 30(a) and 31(a). It is noted that the angle overshoot increased as the speed of the payload increased. The faster the payload speed the longer before setting and the higher the fluctuation in the tilt angle.

For such levels of payload speed, there was no effect on the cart displacement as noted in Figures 29(b), 30(b) and 31(b). The control signal is presented in Figures 29(c), 30(d) and 31(d).). It is noted that changing the payload speed had a very limited effect on the controller output signal especially at lower speeds. However, the effect was more noticeable at higher speeds.

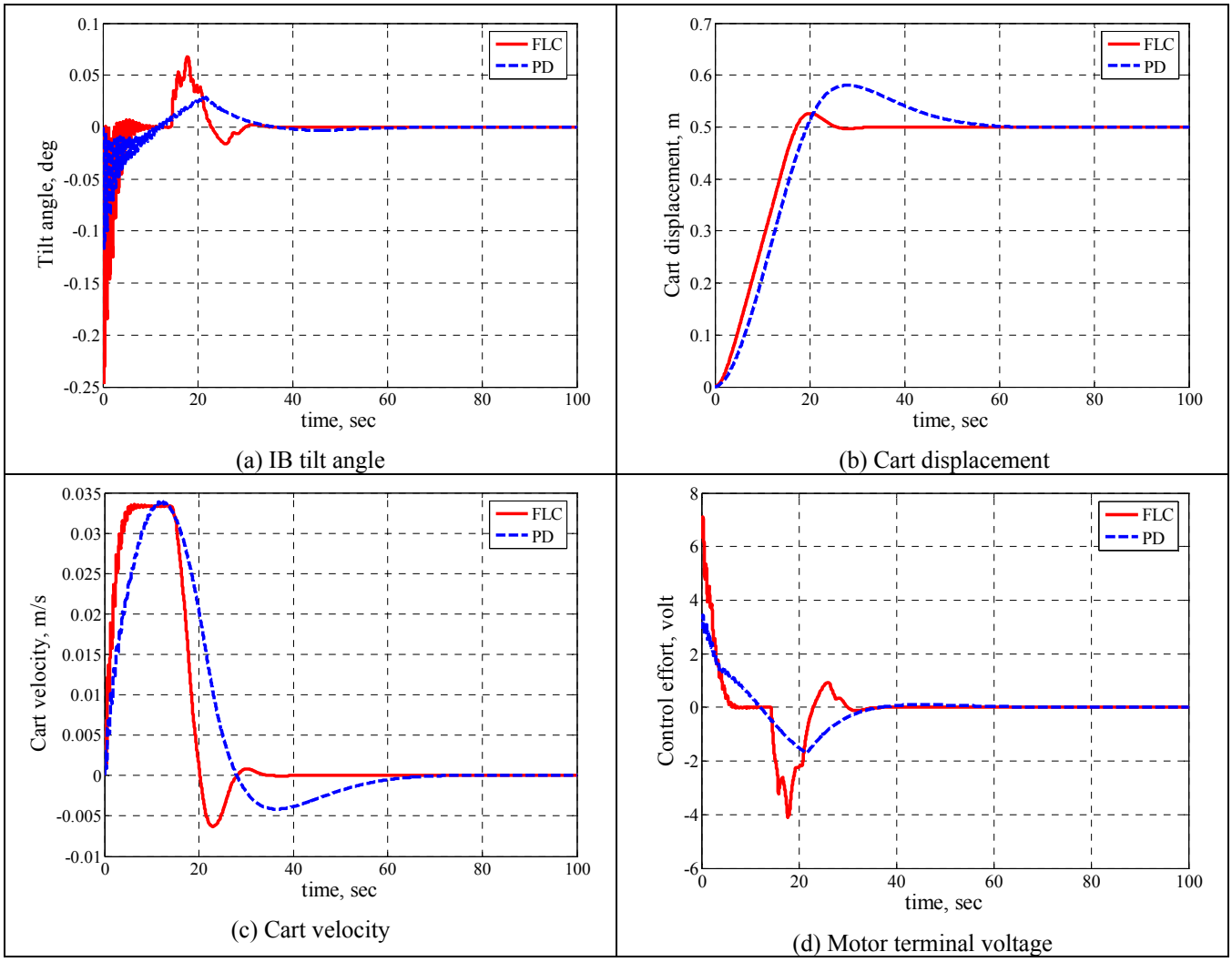

Figure-30. Simulation results (*F = 0 N, f = 0.1 Hz*).

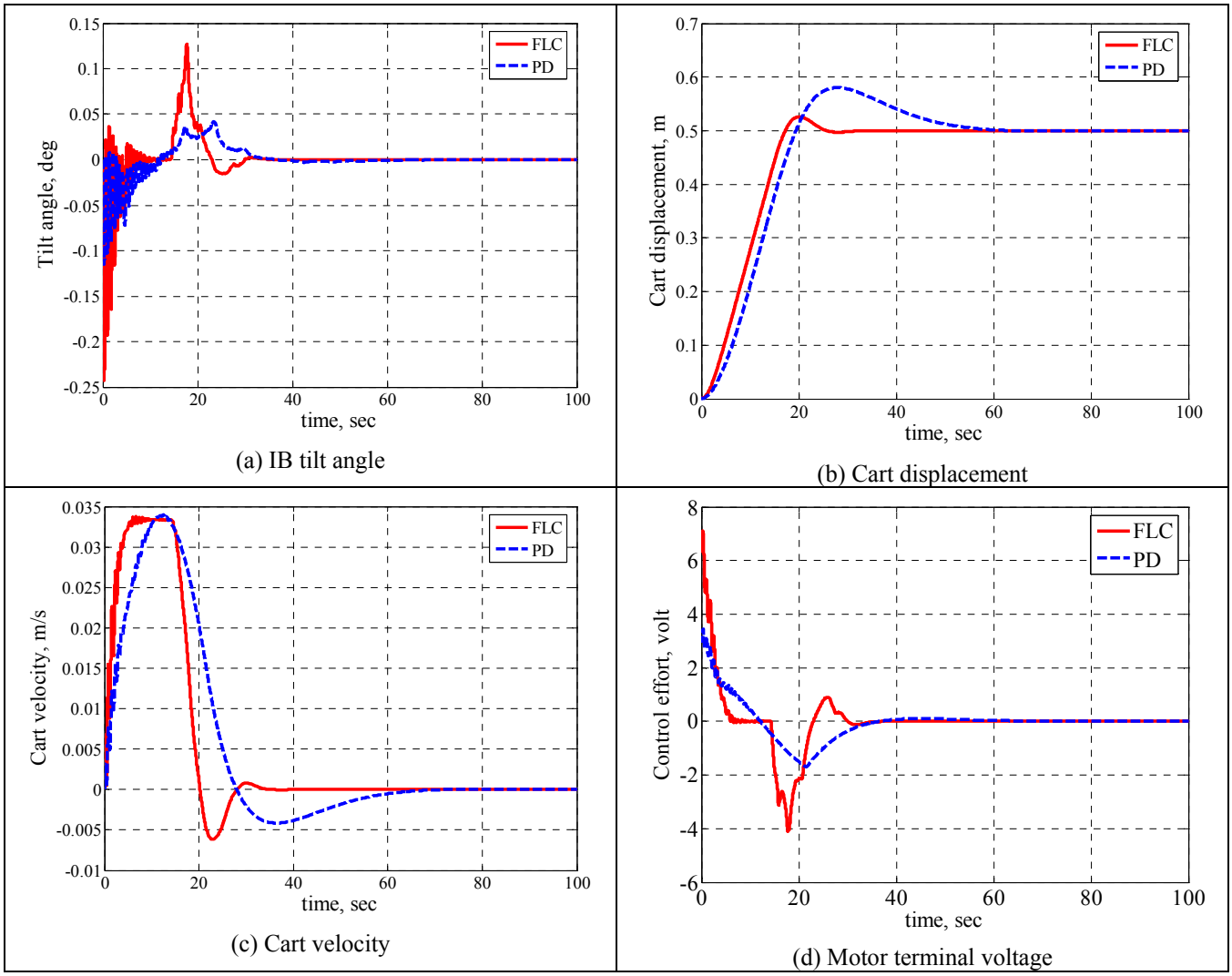

Figure-31. Simulation results (*F = 0 N, f = 1 Hz*).

4.2.6 Effect of rod length

The effect of length of the intermediate body is investigated in this section. The system performance alongside the control signal is presented utilising two different lengths of the IB. As noted in Figure-32 the shorter the IB the harder the balance; short rods lead to high fluctuations of the rod about the upright balance position and long periods of oscillations until settling down. However changing the IB length, with such values, did not affect the linear motion of the vehicle. Changing the IB length corresponds to the position of the rod centre of mass which becomes closer to the vehicle centre point with shorter rods.

5. CONCLUSIONS

A mathematical model of a TWRM system has been developed in planar coordinate frame. An external disturbance force has been applied to the IB, and a payload has been attached to the rod. Two control techniques; PD and PD-like fuzzy control have been developed and implemented to balance the TWRM. Simulations have been carried out to address the effect of applying a disturbance force on the system with attached payload at different locations along the IB. The system dynamic behaviour has been presented alongside the control effort for achieving the required performance in those different cases. Simulations have been carried out for different cases of changing two variables namely; the level and duration of a disturbance force and the position and speed of the payload.

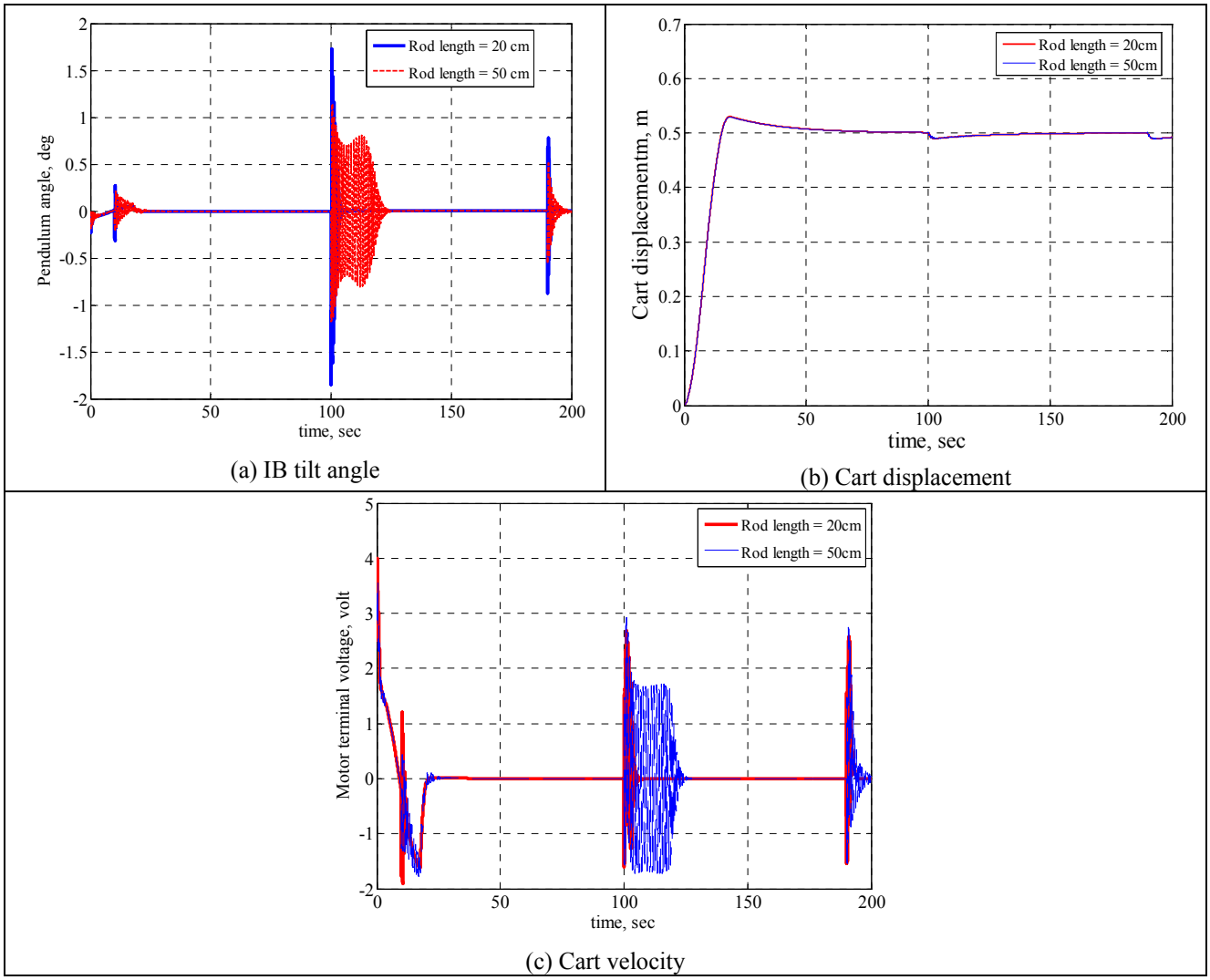

Figure-32. System performance and control signal (Different IB lengths), PD control.

Several observations have been made from the system dynamic equations and have been proved using simulations. Those observations can be summarised as follows:

A disturbance force directly affects balancing of the IB in the upright position; Increasing the disturbance force tends to increase the deviation of the IB from the target balance position. Moreover, the disturbance force acts as drag on the entire system, specifically if applied close to the IB lower end, which tends to decelerate the vehicle and in turn increase the energy consumption of the system.

The position of the disturbance has been shown to be a matter of concern. The results can be stated as:

- If $S > 2L_g$ (force applied above the location of the *COM*) then the effect will be to increase the amount of deviation from the target location
- If $S < 2L_g$ (force applied below the location of the *COM*) then the effect will be to help the controller to achieve balance by decreasing the deviation in the tilt angle.

Thus, the higher the level at which the force is applied the easier it is to balance the IB and the longer the time it takes the vehicle to settle down. Increasing the control efforts V_L and V_R has the effect of increasing the deviation in the tilt angle of the IB and accelerating the entire system out of the target. Increasing the inertia of the various system components tends to add more damping to the system and decrease possible oscillations. However, it will require a lot of control effort to manoeuvre the vehicle and hence more energy consumption.

In conclusion, multiple conditions can result in increasing the complexity of the control system in balancing the TWRM: COM close to the vehicle centre point (IB lower end), disturbance force applied close to that end, shorter IB, higher level of disturbance force, longer period of disturbance effect or high payload speed. Based on the results achieved, it is concluded that the developed control algorithm coped well in those cases with different limits for such disturbances and objectives of the study were met to a great extent.

Further studies will investigate the effect of changing the direction of applying the disturbance force

on system behaviour and develop the mechanical adjustments for the vehicle for safe operation during such cases. The design of control algorithms to deal with various unexpected external disturbances acting on the system is another area of future interest.

Appendices

Linear model of the DC motor

Motor torque

$$\tau_m = k_m i \tag{A1}$$

Back electro magnetic force (EMF) V_e:

$$V_e = k_e \omega \tag{A2}$$

Kirchhoff's voltage Law of the DC motor:

$$V_a - Ri - L\frac{di}{dt} - V_e = 0 \tag{A3}$$

Equation of motion for the motor:

$$\sum M = \tau_m - k_f - \tau_a = I_R \frac{d\omega}{dt} \tag{A4}$$

$$\frac{di}{dt} = \frac{R}{L} i + \frac{k_e}{L} \omega + \frac{V_a}{L} \tag{A5}$$

$$\frac{d\omega}{dt} = \frac{k_m}{I_R} i - \frac{k_f}{I_R} - \frac{\tau_a}{I_R} \tag{A6}$$

Non-Linear Model of the wheels and the IB

Wheels Dynamics

Translational equilibrium of the wheels:

$$\sum F_{y_R} = M_w \ddot{y}_R$$

$$M_w \ddot{y}_R = H_{TR} - H_{FR} - H_R \tag{A7}$$

$$\sum F_{z_R} = M_w \ddot{z}_R$$

$$M_w \ddot{z}_R = V_{TR} - V_R - M_w g \tag{A8}$$

Rotational equilibrium of the wheel around its centre point O_R:

$$\sum M = J_{wx} \ddot{\phi}_{Ry}$$

$$J_{wx} \ddot{\phi}_{Ry} = T_R + H_{FR} R_w - H_{TR} R_w \tag{A9}$$

From motor dynamics, the torque driving the right wheel can be expressed as:

$$T_L = -\frac{K_m K_e}{R R_w} \dot{y}_L + \frac{K_m}{R} V_L \tag{A10}$$

$$T_R = -\frac{K_m K_e}{R R_w} \dot{y}_R + \frac{K_m}{R} V_R \tag{A11}$$

Substituting for T_R from Equation (A11) into Equation (A9) yields:

$$J_{wx} \ddot{\phi}_{Ry} = -\frac{K_m K_e}{R R_w} \dot{y}_R + \frac{K_m}{R} V_R + (H_{FR} - H_{TR}) R_w \tag{A12}$$

$$M_w \ddot{y}_R = -\frac{K_m K_e}{R R_w} \dot{y}_R + \frac{K_m}{R} V_R - \frac{J_{wx}}{R_w} \ddot{\phi}_{Ry} - H_R \tag{A13}$$

$$M_w \ddot{y}_L = -\frac{K_m K_e}{R R_w} \dot{y}_L + \frac{K_m}{R} V_L - \frac{J_{wx}}{R_w} \ddot{\phi}_{Ly} - H_L \tag{A14}$$

Linear transformations:

$$\ddot{y}_R = R_w \ddot{\phi}_{Ry}, \ \ddot{y}_L = R_w \ddot{\phi}_{Ly} \tag{A15}$$

Linear motion of centre of mass of the right and left wheels:

$$\left(M_w + \frac{J_{wx}}{R_w^2}\right) \ddot{y}_R = -\frac{K_m K_e}{R R_w} \dot{y}_R + \frac{K_m}{R} V_R - H_R \tag{A16}$$

$$\left(M_w + \frac{J_{wx}}{R_w^2}\right) \ddot{y}_L = -\frac{K_m K_e}{R R_w} \dot{y}_L + \frac{K_m}{R} V_L - H_L \tag{A17}$$

Intermediate body dynamics

Consider Figures A1 and A2 which represent the free body diagrams of the IB with an external applied disturbance force F. Applying the Newton's second law of motion in the Y direction yields

$$\sum F_Y = (M + M_p) \ddot{Y}$$

$$(H_R + H_L) = (M + M_p)\left(\ddot{Y} + L_g \ddot{\theta}_p \cos\theta_p - L_g \dot{\theta}_p^2 \sin\theta_p\right) + F \tag{A18}$$

Considering the sum of the applied forces in a direction perpendicular to the rod gives,

$$\sum F_{\perp IB} = (M + M_p)\, \ddot{Y} \cos\theta_P$$

$$\begin{aligned}(H_R + H_L)\cos\theta_p + (P_R + P_L)\sin\theta_p - (M + M_p)\left(g\sin\theta_p + L_g \ddot{\theta}_p\right) - F\cos\theta_p \\ = (M + M_p)\ddot{Y}\cos\theta_p\end{aligned} \tag{A19}$$

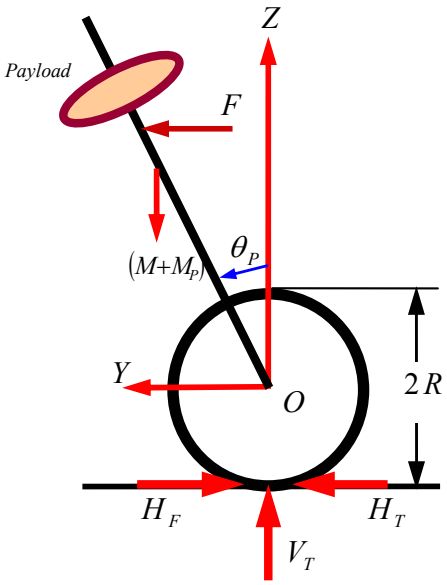

Figure-A1. Schematic diagram of the vehicle.

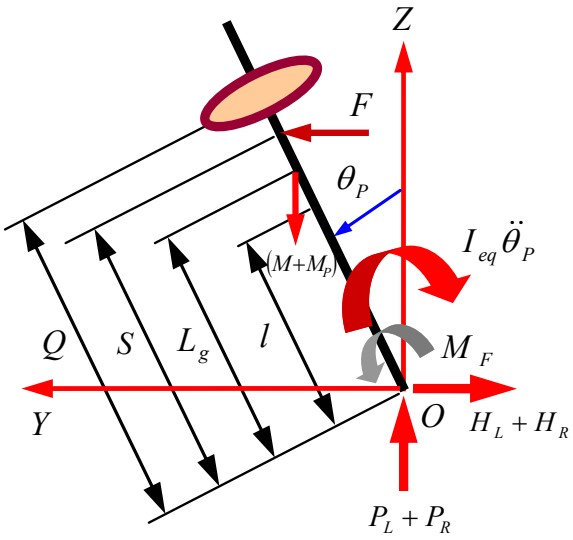

FigureA2. Schematic diagram of the IB.

Finally, equating the sum of the applied moments including the frictional moment at the joint connecting the IB and axle around the global centre of mass yields,

$$\sum Moments_O = I_{eq}\ddot{\theta}_p$$

$$[(H_L+H_R)\cos\theta_P+(P_L+P_R)\sin\theta_P]L_g-(T_R+T_L)-M_F - F\cos\theta_p(S-L_g)=I_g\ddot{\theta}_p \quad \text{(A20)}$$

$$M_F = c_c\dot{\theta}_p + c_v\sin\dot{\theta}_p \quad \text{(A21)}$$

$$T_L+T_R=-\frac{K_mK_e}{RR_w}(\dot{y}_L+\dot{y}_R)+\frac{K_m}{R}(V_L+V_R) \quad \text{(A22)}$$

$$[(H_L+H_R)\cos\theta_P+(P_L+P_R)\sin\theta_P]L_g=I_g\ddot{\theta}_p-\frac{K_mK_e}{RR_w}(\dot{y}_R+\dot{y}_L) \quad \text{(A23)}$$
$$+\frac{K_m}{RR_w}(V_L+V_R)+F\cos\theta_p(Z-L_g)+M_F$$

$$\ddot{Y}=\ddot{Y}_L+\ddot{Y}_R \quad \text{(A24)}$$

Nomenclature

H_{FR} and H_{FL}	Frictional forces between the wheel and the ground
H_{TR}, H_{TL}	Horizontal reaction forces
V_{TR} and V_{TL}	Vertical reaction forces
H_R, H_L	Horizontal reaction forces between the IB and wheel axle
P_R, P_L	Vertical reaction forces between the IB and wheel axle
M_w	Mass of the vehicle wheel
$\ddot{\theta}_P$	Angular acceleration of the IB around X-axis
$\ddot{Y}$	Linear acceleration of the centre point O of the vehicle
F_{z_R}	Resultant force acting on the right wheel in the Z-direction
F_{y_R}	Resultant force acting on the right wheel in the Y-direction
F	External applied disturbance force
$\ddot{Y}$	Linear acceleration of the centre point O of the vehicle.
M_F	Frictional moment at the joint connecting the IB and the wheel axle
c_c and c_v	Coulomb and viscous friction coefficients respectively
V_L and V_R	System input voltage
V_a	Applied voltage
k_m	Proportional constant.
k_e	Back EMF constant
τ_m	Motor produces a torque
I_R	Armature inertial load
V_a	Applied voltage
τ_a	Applied torque
θ	Angular displacement of motor shaft
ω	Angular velocity of motor shaft

REFERENCES

[1] Browning B., Rybski P. E., Searock J. and Veoso M. M. 2004. Development of a soccer-playing dynamically-balancing mobile robot. Proceedings of the International Conference on Robotics and Automation, New Orleans, LA.

[2] D'Andrea R. and Earl M. G. 2005. Design and implementation of a minimum time transition for an inverted pendulum. Proceedings of the Asian

Conference on Industrial Automation and Robotics, Bangkok, Thailand.

[3] Goher K. M. K. and Tokhi M. O. 2008. Modelling, simulation and balance control of a two-wheeled robotic machine with static variation in load position. Proceedings of the 22nd European Conference on Modelling and Simulation**,** Nicosia, Cyprus.

[4] Goher K. M. K. and Tokhi M. O. 2008. Robust control of a two-wheeled robotic machine. Proceedings of the 8th Portuguese Conference on Automatic Control, Vila Real, Portugal.

[5] Goher K. M. K. and Tokhi M. O. 2008. Balance control of a TWRM with a static payload. Proceedings of the 11th International Conference on Climbing and Walking Robots and the support Technologies for Mobile Machines (CLAWAR 2008), The University of Coimbra, Coimbra, Portugal.

[6] Goher K. M. K. and Tokhi M. O. 2008. Balance Control of a TWRM with a Dynamic Payload. Proceedings of the 11th International Conference on Climbing and Walking Robots and the support Technologies for Mobile Machines (CLAWAR 2008), The University of Coimbra, Coimbra, Portugal**.**

[7] Hladek D. 2007. Multi-agent fuzzy control of the robotic soccer. Proceedings of the 5th Slovakian-Hungarian Joint Symposium on Applied Machine Intelligence and Informatics, Popard, Slovakia.

[8] Ibrahim U. F. S. U., Azlan C. A., Abo Osman N. A. and Saifizul A. A. 2006. Intelligent control of self-erecting inverted pendulum via adaptive neuro-fuzzy inference system. American Journal of Applied Sciences. 3(4): 1795-1802.

[9] Ishikawa S. 1991. A Method of indoor mobile robot navigation by fuzzy control. Proceedings of the IEEE/RSJ International Workshop on Intelligent Robots and Systems. (Intelligence for Mechanical Systems), Osaka, Japan.

[10] Kawaji S. and Maeda T. 1991. Fuzzy servo control system for an inverted pendulum. Proceedings of the Internet Fuzzy Engineering Symposium. 2: 812-823.

[11] Kim Y., Kim H. K. and Kwak Y. K. 2005. Dynamic analysis of a nonholonomic two-wheeled inverted pendulum robot. Journal of Intelligent and Robotic Systems. 44(1): 25-44.

[12] Kim Y., Kim H. K. and Kwak Y. K. 2006. Improving driving ability for a two-wheeled inverted pendulum-type autonomous vehicle, Part D: Journal of Automobile Engineering. 220(2): 165-175.

[13] Lee T. H., Leung F. H. F. M., Tam P. K. S. 1999. Position control for wheeled mobile robot using a fuzzy controller. Proceedings of the 25th annual conference of the IEEE Industrial Electronics Society, San Jose, California, USA.

[14] Mamdani E. H. and Assilian S. 1974. Application of fuzzy algorithms for control of simple dynamic plant. Proceedings of IEE, Part D: 121(12): 1585-1588.

[15] Mamdani E. H., Assilian S. 1975. An experiment in linguistic synthesis with a fuzzy logic controller. International Journal of Man-Machine Studies. 7(1): 1-13.

[16] Maravall D., Zhou C. and Alonso J. 2005. Hybrid fuzzy control of the inverted pendulum via vertical forces. International Journal of Intelligent Systems. 20: 195-211.

[17] Marzi H. 2005. Multi input fuzzy control of an inverted pendulum using an armature controlled DC Motor, Robotica. 23(6): 785-788.

[18] Pathak K., Franch J. and Agrwal S. K. 2005. Velocity and position Control of a Wheeled Inverted Pendulum by Partial Feedback Linearization. IEEE Transactions on Robotics. 21(3): 505-513.

[19] Pawlowski S., Dutkiewicz P., Kozlowski P., Wroblewski W. 2001. Fuzzy logic implementation on mobile robot control. The 2nd Workshop on Robot Motion and Control. pp. 65-70.

[20] Piegat A. 2006. What is not clear in fuzzy control systems? International Journal Applied Mathematics and Computer Science. 16(1): 37-49.

[21] Saifizul A. A., Zainon Z., Abu Osman N. A., Azlan C. A. and Ungko Ibrahim U. F. S. 2006. Intelligent control for self erecting inverted pendulum via adaptive neuro-fuzzy inference system. American Journal of Applied Sciences. 3(4): 1795-1802.

[22] Salerno A., Angles J. 2004. The control of semi-autonomous self balancing two-wheeled quasiholonomic mobile robot. Proceedings of the 15th CISM-IFToMM Symposium on Robot Design, Montreal, Canada.

[23] Shi E. X., Huang W. E. and Ling Y. Z. 2004. Fuzzy predictive control of wheeled mobile robot based on multi-sensors. Proceedings of the 3rd International Conference on Machine Learning and Cybernetics, Shanghai, China.

[24] Sun Y. L., Er M J. 2004. Hybrid fuzzy control of robotic systems. IEEE Transactions on Fuzzy Systems. 12(6): 755-765.

[25] Tsai C. C., Lin S. C. and Luo W. L. K. 2006. Adabtive steering of a self-balancing two-wheeled transporter. Proceedings of the Automatic Control Conference, Tamsui, Taiwan.

[26] Tsai M. C. and Hu J. S. 2006. Robust control of auto-balancing two-wheeled cart motion pilot. Proceedings of the Automatic Control Conference, Tamsui, Taiwan.

[27] http://www.segway.com/.

[28] http://leiwww.efpl.ch/joe.

[29] http://www.ibotnow.com/ibot-in-action.html.